Journal of Medicinal Chemistry

pubs.acs.org/jmc Article

Structure-Based Optimization and Discovery of M3258, a Specific Inhibitor of the Immunoproteasome Subunit LMP7 (β5i)

Markus Klein,* Michael Busch, Manja Friese-Hamim, Stefano Crosignani, Thomas Fuchss, Djordje Musil, Felix Rohdich, Michael P. Sanderson, Jeyaprakashnarayanan Seenisamy, Gina Walter-Bausch, Ugo Zanelli, Philip Hewitt, Christina Esdar, and Oliver Schadt

Cite This: *J. Med. Chem.* 2021, 64, 10230−10245 Read Online

ABSTRACT: Proteasomes are broadly expressed key components of the ubiquitin-dependent protein degradation pathway containing catalytically active subunits (β1, β2, and β5). LMP7 (β5i) is a subunit of the immunoproteasome, an inducible isoform that is predominantly expressed in hematopoietic cells. Clinically effective pan-proteasome inhibitors for the treatment of multiple myeloma (MM) nonselectively target LMP7 and other subunits of the constitutive proteasome and immunoproteasome with comparable potency, which can limit the therapeutic applicability of these drugs. Here, we describe the discovery and structure-based hit optimization of novel amido boronic acids, which selectively inhibit LMP7 while sparing all other subunits. The exploitation of structural differences between the proteasome subunits culminated in the identification of the highly potent, exquisitely selective, and orally available LMP7 inhibitor **50** (M3258). Based on the strong antitumor activity observed with M3258 in MM models and a favorable preclinical data package, a phase I clinical trial was initiated in relapsed/refractory MM patients.

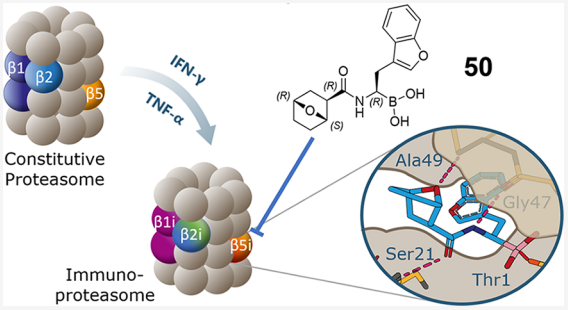

INTRODUCTION

Proteasomes are large multicatalytic complexes that are central components of the cellular machinery for maintenance of protein homeostasis.[1−3] The barrel-shaped 20S core particle of proteasomes consists of 28 subunits assembled in four rings of seven subunits each. The core particle of the broadly expressed constitutive proteasome (cP) contains the distinct proteolytic subunits β1 (*PSMB6*), β2 (*PSMB7*), and β5 (*PSMB5*), which possess caspase-like, trypsin-like, and chymotrypsin-like proteolytic activity, respectively. The differential substrate preferences of each subunit enable the processing of diverse ubiquitinated proteins in cells. A distinct core proteasome particle called the immunoproteasome (iP) contains the unique proteolytic subunits β1i (LMP2 and *PSMB9*), β2i (MECL1 and *PSMB10*), and β5i (LMP7 and *PSMB8*) with chymotrypsin-like, trypsin-like, and chymotrypsin-like activity, respectively. The iP is predominantly expressed in cells of hematolymphoid origin[4−7] and can be induced in other cell types by exposure to inflammatory stimuli such as IFNγ or TNFα.[8]

Aside from its essential function in the maintenance of protein homeostasis, the iP also degrades pathogenic proteins and generates peptidic fragments, which are more efficiently loaded on the class I major histocompatibility complex (MHC I) for antigen presentation compared to cP-derived peptides.[2] Furthermore, the iP-specific proteolytic subunits, in particular LMP7, play an essential role in restoring homeostasis in cells under elevated proteotoxic or oxidative stress.[9]

The essentiality of proteasomes for the viability of multiple myeloma (MM) cells has been underpinned by the approval and wide application of the proteasome inhibitors bortezomib, carfilzomib, and ixazomib. These drugs interfere with the activity of multiple cP and iP proteolytic subunits.[10] While this nonselective mechanism delivers robust clinical efficacy in MM, it is also associated with diverse toxicities including thrombocytopenia, neutropenia, and cardiotoxicity,[10] which can lead to dose reductions, less frequent regimens, or cessation of treatment and thus limit the therapeutic potential of these drugs.[11−14] The restricted expression and unique functional features of iP-specific subunits have led to considerable interest in the potential of selective iP inhibitors in diverse disease settings.[3,12,15] Recent reports have suggested that therapeutic efficacy in preclinical models of inflammation and autoimmunity requires dual inhibition of the iP subunits LMP2 and LMP7.[15−18] However, in the case of preclinical

Received: April 1, 2021
Published: July 6, 2021

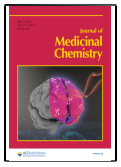

https://doi.org/10.1021/acs.jmedchem.1c00604
J. Med. Chem. 2021, 64, 10230−10245

Table 1. Overview of Subunit-Specific *In Vitro* Biochemical IC_{50} Values of Previously Published Reference Compounds (β5i = LMP7)[a]

Compound	Structure	β1i IC_{50} [nM]	β2i IC_{50} [nM]	β5i IC_{50} [nM]	β1 IC_{50} [nM]	β2 IC_{50} [nM]	β5 IC_{50} [nM]
Bortezomib **1**	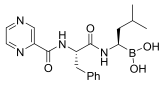	2.9 ±5.5	1630 ±487	1.3 ±0.9	25 ±8.9	12769 ±4971	3.2 ±1.5
Ixazomib **2**	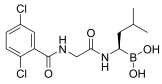 citrate	2.7 ±1.6	4874 ±707	2.9 ±2.3	64[b]	>30000	5.0 ±2.5
Carfilzomib **3**	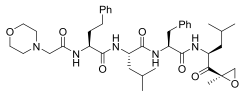	69 ±98	13 ±6.9	3.2 ±1.1	890[b]	43 ±18	2.1 ±0.9
4	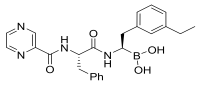	11 ±5.1	4000[b]	1.7 ±0.7	8500[b]	>30000	41 ±16

[a]Assay data represent the mean of a minimum of three determinations including the standard deviation. [b]Single measurement.

cancer models, the therapeutic effects of inhibition of individual iP proteolytic subunits or multiple subunits remain less well characterized, with most preclinical reports to date only describing the activity of dual LMP2/7 inhibitors or compounds with only partial selectivity against the cP subunit β5.[19−25]

The work published in this paper is based on the hypothesis that selective LMP7 inhibition could potentially achieve antitumor activity in B cell-derived malignancies.[3,12,13] Although in recent years substantial progress has been made in the design of selective LMP7 inhibitors, to our knowledge, no compound has been published to date, which has properties enabling oral administration, in order to evaluate this hypothesis. We have generated highly potent LMP7 inhibitors that demonstrate exquisite selectivity against all other proteolytic subunits of the iP and cP. Compound **50** (M3258) also demonstrated an attractive overall profile with regard to physicochemical and drug metabolism and pharmacokinetic (DMPK) properties and delivered robust *in vivo* efficacy and target inhibition in an MM xenograft model. These data supported the recent initiation of a phase I clinical trial of M3258 in relapsed/refractory MM patients (NCT04075721).

RESULTS AND DISCUSSION

As a starting point, we evaluated the subunit inhibition profiles of the clinically approved proteasome inhibitors bortezomib, ixazomib, and carfilzomib (Table 1). The inhibition of each proteolytic subunit of iP (β1i, β2i, and LMP7) and cP (β1, β2, and β5) was determined using fluorescence intensity assays applying specific substrates that undergo cleavage by the individual proteasome subunits. According to our data and in line with previous reports,[26,27] bortezomib and ixazomib displayed comparable subunit specificity with the highest activity against β1i, LMP7, and β5. In contrast, carfilzomib turned out to be less selective, inhibiting not only β1i, LMP7, and β5 but also β2i and β2 proteolytic activity. Each of these inhibitors contains an isobutyl group, which occupies the S1 pocket adjacent to the catalytically active site as a common motif.

Although the iP and cP possess overlapping substrate specificities, it is well established that the iP has a stronger preference for hydrophobic amino acids like tryptophan binding to S1 and is more effective in cleaving such substrates.[28] In contrast, the cP displays a greater preference for cleavage following smaller and polar amino acid residues. Crystallographic investigations from Huber et al. suggested that LMP7 has a larger S1 pocket than β5 due to a Met45 conformation that allows access of sterically demanding groups to the binding pocket.[29] We speculated that these differences could possibly be exploited to generate more selective iP inhibitors. Furthermore, rationally designed LMP7-specific substrates, like (Ac-ANW)2R110 or Ac-ANW-AMC[30] containing a tryptophan to fill the S1 pocket, underline the ability of the S1 pocket to accommodate large bicyclic moieties. Very recently, the reported structures of the cP and chimeric immuno-constitutive proteasome variants in yeast and the electron microscopy report of the human iP[31] have been complemented by the crystal structure of an α-aminoboronic acid derivative in complex with the *bona fide* human iP,[17] in which a large 2,4-dimethylphenyl moiety fills the S1 pocket.

Cocrystal Structure of Compound 4 with the iP. Since this information was unknown at the time at which we initiated our drug discovery program some years ago, our initial efforts focused on generating insights into the human iP structure. We were able to generate a cocrystal structure of the human iP with compound **4** (Table 1), which is a bortezomib derivative synthesized similar to reported methods.[32] Instead of an isobutyl group, **4** contains a more sterically demanding 3-ethyl-substituted benzyl moiety (Figure 1). Although **4** displayed

https://doi.org/10.1021/acs.jmedchem.1c00604
J. Med. Chem. 2021, 64, 10230−10245

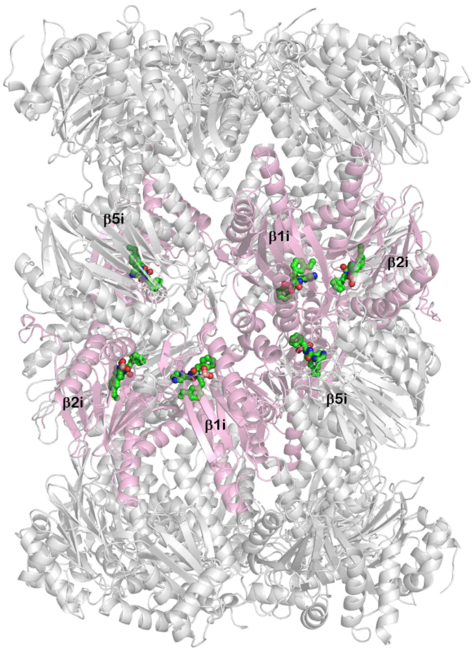

The structure of the human 20S iP in complex with compound **4** to 2.84 Å resolution was solved (PDB ID: **7B12**). The quaternary structure of the human iP indicates the typical elongated cylindrical shape of 20S proteasome core particles with the 28 subunits arranged in four heptameric rings as a α7β7β7α7 sandwich (see Figure 1). Compound **4** is bound covalently to all six of the proteolytic subunits (β1i, β2i and β5i, in pink) with nearly identical binding modes.

Figure 1. Human iP (S20 core particle) X-ray structure in complex with compound **4**.

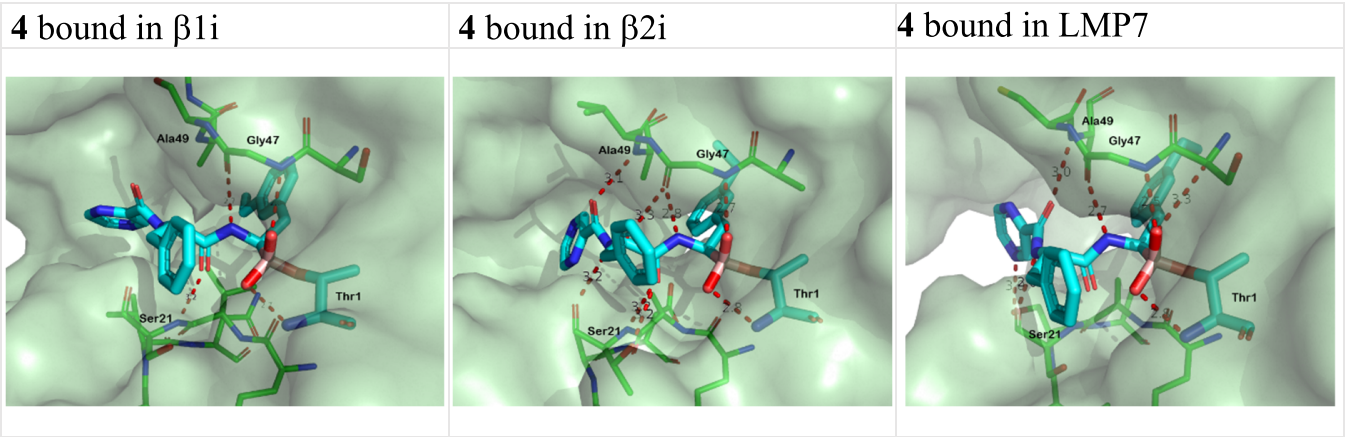

Figure 2. Binding modes of **4** in *β*1i, *β*2i, and LMP7. The orientation of the ethyl-phenyl moiety in *β*1i is flipped by roughly 180° compared to that in *β*2i and LMP7. The hydrogen bonding network of compound **4** with the catalytic subunits is mostly built in an antiparallel *β*-sheet manner, interacting with the protein main chain in the substrate binding channel. The pyrazine group of **4** binds into the S3 pockets of the catalytic subunits, adopting several ring orientations, depending on the subunit type and on the neighboring protein chains.

Scheme 1. Strategy to Increase LMP7 Specificity

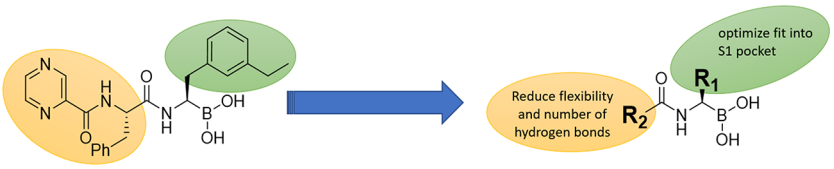

different potencies against *β*1i, *β*2i, and LMP7, in the crystal structure, all subunits were found to be occupied, likely as a result of the high concentration used during cocrystallization (Figure 2). In each case, the boron atom covalently interacted with the nucleophilic oxygen lone pair of Thr1 and led to the formation of a tetrahedrally coordinated boronate adduct as expected. In the LMP7 subunit, the large 3-ethylphenyl group, replacing the isobutyl group of bortezomib, nicely filled the S1 pocket.

Compound **4** showed ∼24-fold biochemical selectivity for LMP7 over *β*5, contrasting to the ∼2-fold selectivity measured with bortezomib (Table 1). Compound **4** contains an identical dipeptide residue, which adopts the known antiparallel *β*-sheet conformation.[33] The amide bond next to the active site is essential for activity and interacts with Ser21 and Gly47 in LMP7 through two strong hydrogen bonds, while the second amide group forms two hydrogen bonds with the peptidic backbone of the LMP7 subunit (Ala49 and Ser21). Similar

https://doi.org/10.1021/acs.jmedchem.1c00604
J. Med. Chem. 2021, 64, 10230−10245

Scheme 2. Synthetic Access to α-Amino Boronic Acid Building Blocks[a]

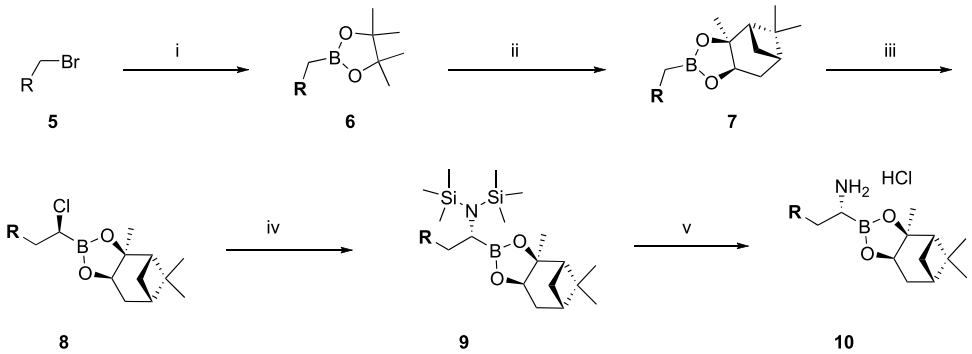

[a]Reagents and conditions: (i) B_2pin_2, Pd(dppf), KOAc, dioxane, 85 °C, 16 h ; (ii) (+)-pinanediole, diethyl ether, room temperature, 16 h; (iii) Matteson homologation: (1) DCM, BuLi, −100 to −78 °C and (2) $ZnCl_2$, −78 to room temperature; (iv) LiHMDS, −78 °C to room temperature, 18 h; (v) HCl in ether, −10 °C to room temperature, 2 h.

Scheme 3. General Synthesis of Pinanediol Boronates; Separation and Deprotection[a]

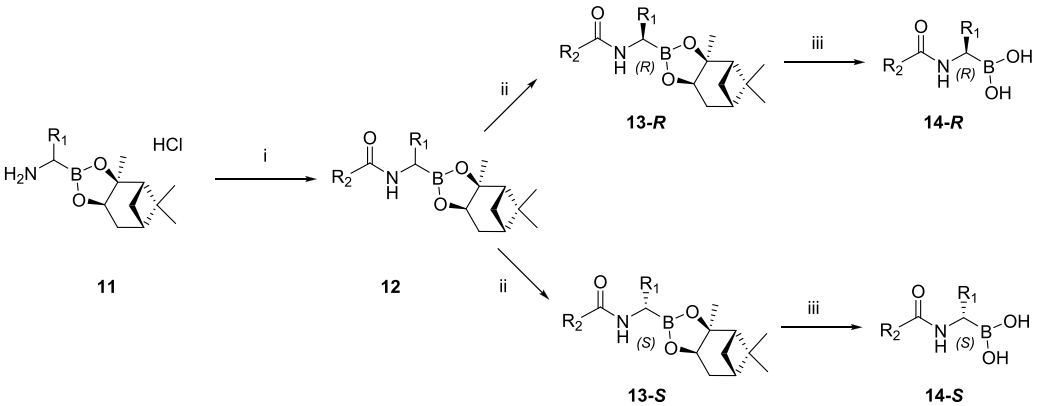

[a]Reagents and conditions: (i) R_2COOH, HATU, DMF, DIPEA, room temperature, 2 h; (ii) chiral SFC separation; (iii) isobutylboronic acid, 2 N HCl, MeOH, pentane.

interactions were identified in β2i (Thr21 replaces Ser21), β1i, and in the β5 subunit of the cP. Despite the significant changes in S1 pocket selectivity, the H-bond network formed by the dipeptide residue of **4** did not result in a pronounced potency difference between subunits.

We therefore hypothesized that LMP7 selectivity could be gained by weakening this hydrogen bonding network and replacing the second amide group (Scheme 1).

In our initial approaches, we replaced R_2 with highly substituted sulfonamides or tertiary amides.[34] However, a balance between LMP7 specificity, good metabolic stability, and sufficient permeability could not be achieved. In order to improve the physicochemical profile and lower tPSA, we moved our focus to R_2 groups containing a reduced number of H donors and acceptors to fill the S2/S3 pockets. Additionally, we aimed to combine these with large R_1 groups to allow for an optimized fit into the S1 pocket.

Synthesis of LMP7 Inhibitors. Since the commercial accessibility of protected α-amino-boronates containing various R-groups is limited, we synthesized these building blocks (Scheme 2) to systematically explore the SAR of the S1 pocket of the iP. Starting from aliphatic, benzylic, or bicyclic methylene bromides **5**, like 3-(bromomethyl)benzofuran, Pd-catalyzed borylation applying established protocols[35] led to the corresponding pinacol boronates **6** in good yields. In order to enable the stereoselective introduction of the chiral α-amino substituent, the pinacol boronates were converted into (+)-pinanediol boronates **7** as a chiral directing group using a transesterification protocol. Matteson homologation[36] applying (dichloromethyl)-lithium at low temperatures (−78 to −100 °C) and anhydrous $ZnCl_2$ as a catalyst led to diastereoselective formation of α-*S*-chloro boronates **8** usually with good stereoselectivity based on GC-analysis. Nucleophilic displacement of the chlorine substituent with *N*-lithiohexamethyldisilazane followed by cleavage of the silyl groups using HCl or trifluoroacetic acid yielded the desired *R*-configured derivatives **10**, in most cases as solid salts, which could be stored at −20 °C without degradation or epimerization.

These α-aminoboronic acid building blocks were then coupled with acids using standard coupling reagents such as HATU to obtain the corresponding amides **12** in good yields (Scheme 3). At this stage, the stereochemical purity could also be readily determined by chiral supercritical fluid chromatography (SFC). In order to further improve the stereochemical purity of the desired *R*-diastereomers and to investigate the activity of the *S*-diastereomers, a chiral separation of both diastereomers was performed on a preparative scale for selected examples. However, the *S*-configured diastereomer proved to be significantly less active on LMP7 than the corresponding *R*-diastereomer. These observations confirm those previously reported by Zhu et al.[32] In all cases investigated, the *R*-configured diastereomers were between

https://doi.org/10.1021/acs.jmedchem.1c00604
J. Med. Chem. 2021, 64, 10230−10245

Table 2. Structures and SAR of Compounds 15−21, Summarizing Substituent Effects on R_1 Groups (β5i = LMP7)[a]

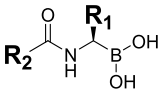

Compound	R_2	R_1	β5i (biochemical) IC_{50} [nM]	β5 (biochemical) IC_{50} [nM]	Ratio β5/β5i	β5i (cellular) IC_{50} [nM]	β5 (cellular) IC_{50} [nM]	Ratio β5/β5i
15			1000 ±120	15000 ±3450	15	3300 ±450	6997 ±283	2.1
16			160 ±340	16000 ±1910	99	643 ±23	9565 ±492	15
17			91 ±6	6300 ±849	69	438 ±57	6287 ±566	14
18			130 ±21	26000 ±1410	194	896 ±113	>30000	>33
19			**85** ±2.8	15000 ±707	**182**	**434** ±21	24454 ±2121	**56**
20			38 ±11	5600 ±495	148	983 ±156	8748 ±212	8.9
21			1200 ±141	>30000	>25	1407 ±495	5900 ±340	4.2

[a]All assay data represent the geometric mean including standard deviation of a minimum of two independent experiments in duplicate.

10- and 100-fold more active on LMP7 and minor amounts of *S*-isomers did not impair the SAR evaluations. Consequently, mixtures containing low amounts of *S*-diastereomers could be readily used in biochemical experiments for determination of IC_{50} values. In our hands, the deprotection of the (+)-pinanediol boronates **13** was most effectively achieved by a biphasic transesterification method applying isobutylboronic acid[37] in order to obtain the free boronic acid derivatives **14** after lyophilization as amorphous powders. Crystalline trimers comparable to those previously reported with bortezomib[38] could be finally obtained by recrystallization.

SAR of R_1 (Tables 2 and 3). We began our SAR exploration of the S1 pocket using compounds containing a benzyl group as R_2 (see Table 2), in which a bending induced by the methylene linker allowed the phenyl moiety to interact with Cys48 in the LMP7 subunit via van der Waals interactions. Despite not being the best choice in terms of potency, benzyl resulted in LMP7/β5 selectivity gains superior to other R_2 groups with longer linkers like ethylene or propylene (data not shown). Direct attachment of phenyl to the amide resulted in a loss of potency.

The first compound of this series (Table 2, **15**) harboring an isobutyl group as R_1 yielded only modest IC_{50} values of 1000 and 15,000 nM against human LMP7 and β5, respectively, indicating that the high activity of bortezomib or ixazomib toward LMP7 is mainly driven by the H-bond interactions of the dipeptidyl moiety in S2/S3. Changing R_1 to benzyl (**16**) led to a 6-fold improvement in potency for LMP7, whereas activity for β5 remained unchanged. Further optimization of the substitution pattern of the phenyl group revealed that small nonpolar substituents like methyl or chloro in para and meta positions further enhanced potency toward LMP7 and resulted in biochemical IC_{50} values below 100 nM (**17**, **19**, and **20**), likely as a result of enhanced lipophilic interactions with the S1 pocket of LMP7. In terms of selectivity, the best ratios were observed for compounds containing either 3,4-dimethyl or 2,4-dimethyl substitution patterns (ratio: >150 for **18** and **19**). While the larger LMP7 S1 pockets nicely accommodated these more sterically demanding moieties, they were not compatible with the more sterically restricted β5 S1 pocket. This resulted in improved LMP7 selectivity for these examples. Similar trends were also observed in proteolytic cleavage assays in A549 cells (cellular β5 assay, Table 1) and human peripheral blood mononuclear cells (PBMCs; cellular LMP7 assay, Table 1) applying specific luminogenic substrates.[30] Although cellular selectivity ratios were generally smaller compared to those observed in biochemical assays, significant selectivity was confirmed for **18** and **19**. As mentioned above, inverting the configuration at the stereocenter reduced both LMP7 activity and selectivity in biochemical and cellular assays, as exemplified by compound **19** versus **21**.

Docking studies with **4** employing our crystal structure suggested that bicyclic aromatic structures may overlay well with the selectivity-maximizing 3,4-dimethylphenyl moiety. Indeed, replacement of the 3,4-dimethyl phenyl in R_1 by 2-benzofuranyl (**22**, Table 3) gave comparable results to **19**. Introduction of a regioisomeric 3-benzo-furanyl group further enhanced LMP7 potency by 10-fold into the single digit nM IC_{50} range and simultaneously improved biochemical selectivity versus β5 to >400-fold (**23**). Notably, **23** also led to a robust increase in LMP7 cellular inhibition into the low two-digit nM range. Encouraged by these results, various other

https://doi.org/10.1021/acs.jmedchem.1c00604
J. Med. Chem. 2021, 64, 10230−10245

Table 3. Structures and SAR of Compounds 22−32 Containing Bicyclic R_1 Groups (β5i = LMP7)[a]

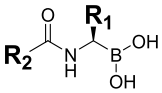

Compound	R_2	R_1	β5i (biochemical) IC_{50} [nM]	β5 (biochemical) IC_{50} [nM]	Ratio β5/β5i	β5i (cellular) IC_{50} [nM]	β5 (cellular) IC_{50} [nM]	Ratio β5/β5i
22	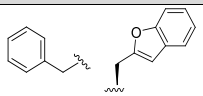		29 ±7.8	5000 ±0	172	824 ±141	10148 ±3385	12
23	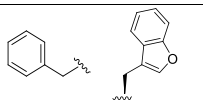		**2.1** ±1.0	900 ±420	**419**	**14** ±7.9	573 ±143	**41**
24	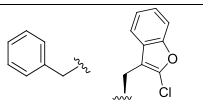		200 ±56.6	20000 ±700	104	824 ±141	16492 ±707	6.8
25	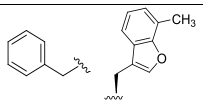		4.5 ±0.6	1200 ±70.7	276	29 ±4.9	2098 ±1461	71
26	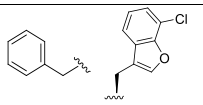		4.1 ±0.4	860 ±106	210	41.5 ±12.1	2062 ±963	49
27	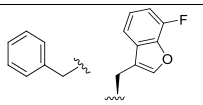		3.1 ±1.2	530 ±57	168	22.8 ±14.2	785 ±196	34
28	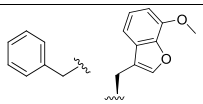		2.2 ±0.1	140 ±0	63	8.9 ±10.4	222 ±29	24
29	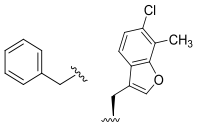		6.4 ±1.7	1700 ±212	272	164 ±21	7325 ±1417	44
30	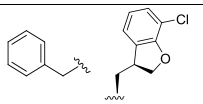		1.8 ±0.3	2900 ±778	1620	25 ±14	6099 ±141	243
31	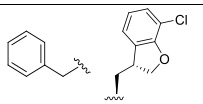		610 ±63	>30000	>49	9670 ±1770	>30000	n.d.
32	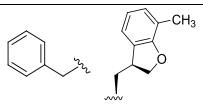		3.1 ±0.7	7200 ±495	2334	53 ±6.3	14000 ±0	262

[a]All assay data represent the geometric mean including standard deviation of a minimum of two independent experiments in duplicates.

bicyclics like 2-naphthalene, 3-naphthalene, 3-benzothiophene, 3-*N*-methylindole, or 3-N-methylindazole (not reported here) were investigated but none of these outperformed the 3-benzofuranyl group in terms of potency and selectivity.

The favorable physicochemical profile (MW, 323 g/mol; tPSA, 83Å^2; log *P*, 3.5; log *D*, 1.0; kinetic solubility, >200 μM) and high metabolic stability in mouse and human liver microsomes qualified **23** for examination of its *in vivo* PK properties. After i.v. application in mice, **23** showed acceptable clearance (CL), volume of distribution (Vss), and half-life ($t_{1/2}$) values of 0.18 L/h/kg, 2.25 L/kg, and 0.37 h, respectively. The oral bioavailability of **23** was 37% when applied at 0.5 mg/kg. Although benzofuranes are commonly considered to be metabolically labile,[39] in the case of **23**, the presence of the nearby polar boronic acid likely prevented oxidative metabolism, which is usually observed for these kinds of electron-rich heterobicycles.

We next examined whether modifications by small substituents could further enhance the selectivity of compounds containing 3-benzo-furanyl. While substituents such as

https://doi.org/10.1021/acs.jmedchem.1c00604
J. Med. Chem. 2021, 64, 10230−10245

chloro were not allowed at the 2-position (exemplified by **24**), F, Cl, Me, or OMe at position 7 (**25**−**28**) or 6 and 7 (**29**) was tolerated but had no significant positive effect on either activity or selectivity. In another approach, we investigated the influence of partial saturation of the oxo heterobicycle and tested both stereoisomers after chiral separation. The *S*-stereoisomer (**31**) failed to fit into the LMP7 S1 pocket and was only weakly active. In contrast, *R*-stereoisomer **30** served as a potent inhibitor of LMP7 activity and showed increased selectivity against β5. Replacing 7-chloro with 7-methyl led to an exquisitely selective compound (**32**) within this subseries, as demonstrated in both biochemical and cellular assays. Of note, this improvement in selectivity was only accompanied by a relatively modest reduction of cellular LMP7 potency compared to **23**.

SAR of R_2 (Tables 4 and 5). Having identified potent and selective R_1 residues, we next shifted our focus toward the optimization of the R_2 group. We maintained the synthetically tractable 3-benzo-furanyl group as R_1 and replaced the phenyl moiety of R_2 with various N-containing mono- or bicyclics (Tables 4 and 5). These retained attractive biochemical potency as exemplified by **33**−**37**. However, unsurprisingly, these modifications reduced biochemical and cellular selectivity toward LMP7, likely as a result of enhanced interactions by the additional H-bond acceptors with the backbone of both the β5 and LMP7 subunits. Intensive efforts to improve LMP7 specificity by introduction of substituents (e.g., halogen, alkoxy, amides, etc.) at the phenyl ring of R_2 had little effect compared to **23**. One of the few exceptions was compound **38** carrying an *ortho*-nitrile group. Combination of this R_2 group with (3*S*)-2,3-dihydro-1-benzofuran-3-yl (**39**) or its 7-chloro (**40**) or 7-methyl (**41**) derivatives as R_1 led to derivatives with impressive biochemical β5 splits (>1000-fold) as well as improved selectivity (>400-fold) in cells. However, despite possessing a good overall physicochemical profile (e.g., compound **39**: MW, 350 g/mol; tPSA, 103 Å^2; log *P*, 1.75; log *D*, 1.3; kinetic solubility, >200 μM) and acceptable metabolic stability in mouse (37 μL/min/mg protein) and human liver microsomes (<10 μL/min/mg protein), an *in vivo* mouse PK study with **39** showed a slightly higher clearance following i.v. application (1.97 L/h/kg) than for compound **23** and a half-life of 0.71 h, while the volume of distribution (*V*ss) was 1.88 L/kg. Bioavailability was found to be 13% when applied at 0.5 mg/kg.

Moving back to the 3-benzo-furanyl group as R_1, we decided to redesign R_2 by switching from flat aromatic groups to three-dimensional saturated moieties containing H-bond acceptors to potentially enable more specific interactions. Surprisingly, the introduction of α- or β-ethers already led to slight improvements in both biochemical LMP7 potency and selectivity (**43** and **44**), which contrasted to alkyl moieties like the acetyl derivative **42**. Based on our crystal structure, this observation can be rationalized by formation of a new H bond between the backbone NH of Ala49 and the ether oxygen (Figure 3A).

Similar effects on potency and selectivity were observed when oxygen was incorporated into the 2- or 3-position of five- or six-membered rings as exemplified by compounds **45**−**48**, while the corresponding purely carbocyclic cyclo-pentyl or hexyl derivatives (data not shown) were only weakly active on LMP7. Based on the docking poses of **47** and **48**, a clear discrimination of the preferred stereochemistry was not predictable and indeed both compounds exhibited similar

Table 4. Structures and SAR of Compounds 23 and 33−41 Containing Heterocyclic and Cyano-Substituted R_2 Groups (β5i = LMP7)[a]

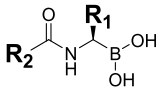

Compound	R_2	R_1	β5i (biochemical) IC_{50} [nM]	β5 (biochemical) IC_{50} [nM]	Ratio β5/β5i	β5i (cellular) IC_{50} [nM]	β5 (cellular) IC_{50} [nM]	Ratio β5/β5i
23			**2.1** ±1.0	900 ±420	**419**	**14** ±7.9	573±143	**41**
33			1.9 ±0.9	410 ±64	212	18.0 ±1.4	328 ±87	18
34			2.3 ±0.7	230 ±35	101	15.5 ±0.7	204 ±219	13
35			2.3 ±0.8	540 ±14	232	24.7 ±5.7	646 ±89	26
36			3.7 ±0.8	770 ±156	212	31.0 ±1.4	894 ±141	29
37			11 ±4.3	2300 ±354	222	71.0 ±2.8	2538 ±353	36
38			5.2 ±0.6	1700 ±71	334	42 ±7.8	2221 ±814	52
39			3.1 ±0.8	2400 ±669	758	20 ±14	2520 ±1223	126
40			2.9 ±0.3	7400 ±1270	2573	51 ±5.0	20904 ±2828	406
41			4.4 ±0.5	14000 ±1410	3147	60 ±2.1	>30000	496

[a]All assay data represent the geometric mean including standard deviation of a minimum of two independent experiments in duplicates.

IC_{50} values in the biochemical LMP7 assay. Productive hydrogen bonding requires orientation of the tetrahydrofuran oxygen toward the peptide bond (formed by Ala49-Cys48). However, this also required the furan system to adopt an energetically unfavorable conformation. Freezing of this bioactive conformation was achieved by incorporation into a bicyclic system like the 7-oxabicyclo[2.2.1]heptane system, which is only rarely used in drug design. Indeed, this approach led to the identification of compounds **49** and **50**, which both exhibit an exo-stereochemistry in the bicyclic system. Compound **50** combined high biochemical potency and selectivity, which translated well into cellular assays. In contrast, the endo isomers **51** and **52**, which do not allow optimal positioning of the ether oxygen, were only moderately active.

The anticipated H-bond formation with the peptidic backbone in the S2 pocket could be confirmed by the generation of an additional cocrystal structure of **50** with the 20S iP, which is shown in Figure 3.[40−42] As a result of the

https://doi.org/10.1021/acs.jmedchem.1c00604
J. Med. Chem. 2021, 64, 10230−10245

Table 5. Structures and SAR of Compounds 42−52 Containing Linear, Cyclic, and Bicyclic Ethers as R_2 Groups (β5i = LMP7)[a]

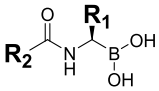

Compound	R_2	R_1	β5i (biochemical) IC_{50} [nM]	β5 (biochemical) IC_{50} [nM]	Ratio β5/β5i	β5i (cellular) IC_{50} [nM]	β5 (cellular) IC_{50} [nM]	Ratio β5/β5i
42			18 ±0.1	1400 ±71	70	27.1 ±6.3	420 ±56	16
43			6 ±2.0	820 ±35	137	26.7 ±5.7	520 ±274	20
44			1.9 ±0.4	400 ±71	205	10.6 ±1.9	241 ±87	23
45			5.9 ±0.6	930 ±92	158	40.0 ±1.1	817 ±375	20
46			190 ±14.1	24000 ±3540	128	400 ±28.3	15000 ±375	38
47			28 ±0.7	5000 ±919	175	55 ±2.1	2996 ±173	54
48			10 ±2.1	4300 ±559	410	13.7 ±6.2	1689 ±323	123
49			15 ±10	6500 ±942	444	19.6 ±11.8	2445 ±386	124
50			**3.6** ±2.4	2500 ±396	**684**	**3.4** ±1.4	1035 ±294	**305**
51			89 ±17.9	15000 ±3310	173	n.d.	n.d.	-
52			140 ±21	>30000	>210	n.d.	n.d.	-

[a]All assay data represent the geometric mean including standard deviation of a minimum of two independent experiments in duplicates.

bicyclic system, conformational changes are highly constrained and prevent interaction between the ether oxygen and the peptidic backbone of the other iP and cP subunits.

Cyclic ethers like THF are known to be prone to CYP-mediated oxidation in the alpha-position[43] and are usually not regarded as desirable structural motifs in drug design. THF derivatives have been even used as prodrugs[44] due to their rapid oxidative cleavage. Indeed, our metabolic studies suggested an elevated oxidative metabolism, which was more pronounced for **45** and **46** and surprisingly low for **47** and **48**.

Notably, the bicyclic ether motif in compounds **49** and **50** was metabolically beneficial despite its slightly higher lipophilicity (Table 6). Improved stability of bicyclic ether amides toward metabolism has also been reported recently for CXCR7 modulators.[45] Additionally, the metabolic stability of compound **50** was confirmed in mouse and human hepatocyte studies, which indicated clearance values of 15 and 6.2 μL/min/10^6 cells, respectively. The incorporation of the alpha-carbon as a bridgehead into a bicyclic system likely prevents its metabolism either due to steric reasons or because the constrained pyramidal conformation does not allow a sufficient stabilization of the radical intermediate that is usually formed during CYP-mediated metabolism.

In addition to its high biochemical (IC_{50} = 3.6 nM) and cellular (IC_{50} = 3.4 nM) potency against the LMP7 subunit, compound **50** was metabolically stable and displayed a favorable physicochemical profile (MW, 329 g/mol; tPSA, 92 Å^2; log *P*, 2.3; log *D*, 1.1; kinetic solubility, >200 μM) and acceptable permeability ($P_{app,AB}$: 8.2 × 10^{-6} cm/s, ER: 2.8). Biochemical assays with each iP and cP proteolytic subunit confirmed the exquisite LMP7 selectivity of **50**, exemplified by the lack of inhibition of β1, β2, β1i, and β2i up to the highest tested concentration of 30 μM and the greatly reduced inhibition of β5 (IC_{50} = 2500 nM; Table 7). Jump dilution experiments revealed a prolonged target occupancy in a range of several hours.[41,42] Based on these attractive features, **50** was chosen for extended *in vitro* selectivity profiling, including a selection of proteases (SI, Table S2) and other safety relevant targets (SI, Table S3). No potent off-target activity in the nanomolar range was observed, and only a few proteases and 5-HT2A were found to be inhibited at micromolar concentrations. In parallel, cell viability was assessed in HepG2 cells and rat and human hepatocytes by ATP depletion (Cell Titer Glo assay at 48 or 72 h). In contrast to bortezomib **1**, compound **50** consistently showed a weak cytotoxicity with IC_{50} values of 48 μM in HepG2 cells, 64 μM in rat hepatocytes, and 91 μM in human primary hepatocytes (SI, Tables S4−S6). Consequently, the cellular split between significant target modulation and initial cytotoxicity is around 10,000-fold. The exquisite *in vitro* profile justified the in-depth *in vivo* characterization of compound **50** in PK and pharmacodynamic (PD) experiments.

***In Vivo* Profiling of Compound 50.** After i.v. application in mice, **50** revealed overall favorable PK characteristics. Values for clearance, volume of distribution, and half-life were determined to be 0.19 L/h/kg (CL), 0.47 L/kg (*V*ss), and 1.71 h ($t_{1/2}$), respectively. The oral bioavailability of **50** was ∼35% when applied at 10 mg/kg (vehicle: 0.25% Methocel/0.25% Tween 20 in PBS). The dose-dependent *in vivo* antitumor activity and *in vivo* inhibition of tumor LMP7 by compound **50** were first evaluated in mice xenografted with the human MM cell line U266B1. When applied daily *per os* at 1 mg/kg, **50** achieved a significant and strong antitumor activity exemplified by sustained tumor regression (Figure 4A).

A lower daily oral dose of 0.3 mg/kg still resulted in significant tumor growth inhibition albeit less pronounced, while 0.1 mg/kg did not significantly affect tumor growth. Each dosing regimen was well tolerated in mice (Figure 4B). U266B1 tumor samples were taken from mice 1 and 6 h following the final application of the vehicle or **50** at 0.3 and 0.1 mg/kg for examination of LMP7 activity as a PD readout (Figure 4C). Consistent with the antitumor effects described above, the 0.3 mg/kg dose of **50** led to a significant reduction of tumor LMP7 activity at 1 and 6 h compared to the control group, while the 0.1 mg/kg group was without significant effect at any time point. The regression of U266B1 tumors under treatment with **50** at 1 mg/kg precluded PD assessments in this experiment. As such, a separate PK/PD experiment was performed using a single oral application of **50** at 1 and 0.3

https://doi.org/10.1021/acs.jmedchem.1c00604
J. Med. Chem. 2021, 64, 10230−10245

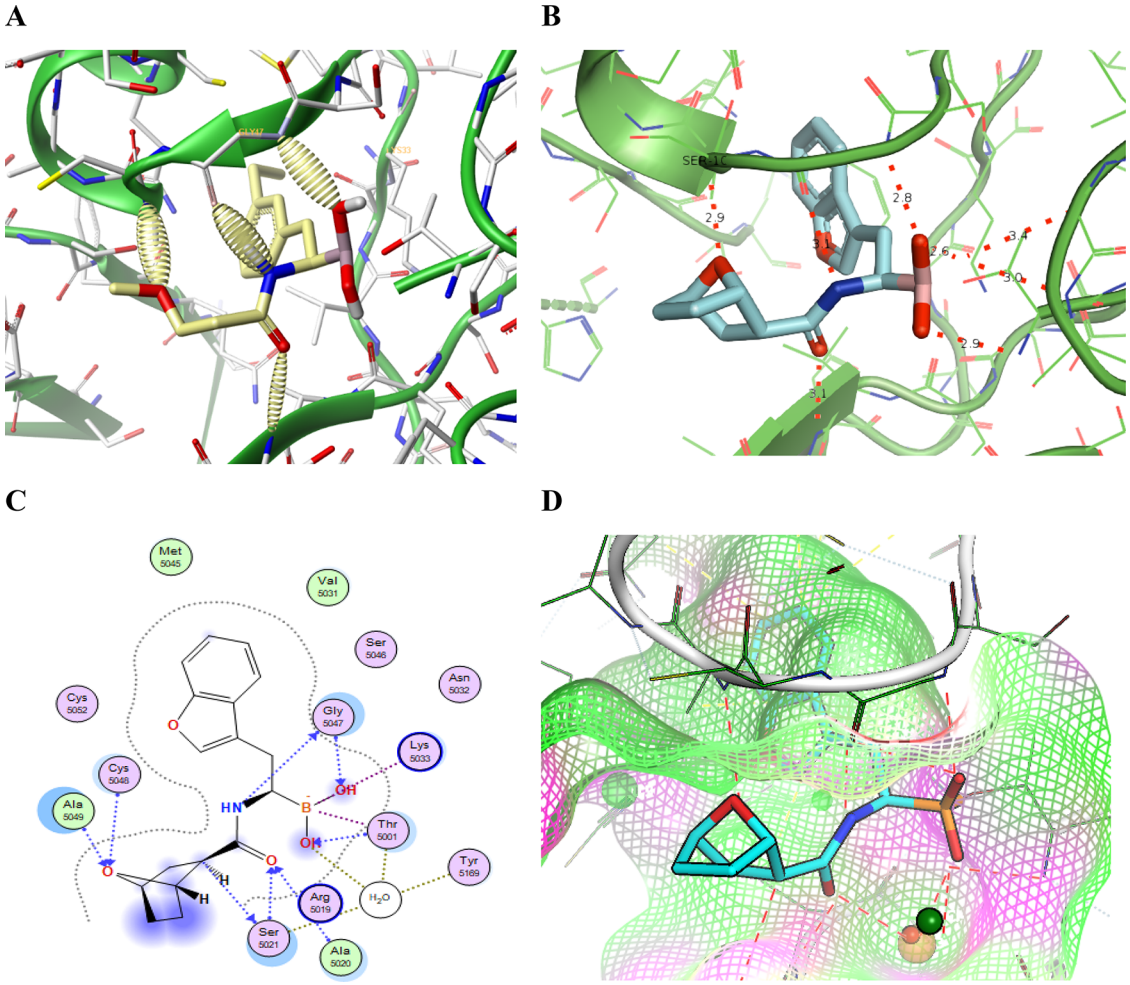

Figure 3. Interactions of **44** and **50**. (A) Anticipated H-bond formation for **44**. H bonds are represented as cylindrical spheres. (B) Crystal structure of **50** (PDB ID: 7AWE). Compound **50** is shown in the LMP7 subunit. (C) Ligand interactions of **50** generated using the MOE program. Relevant interactions are indicated by dashed lines. (D) Graphical illustration of the surface of the LMP7 pocket. Green and magenta indicate lipophilic and polar surfaces, respectively.

Table 6. CLint Data and log *P* of Compounds 45−50

compound	45	46	47	48	49	50
liver microsome CLint (m/h) [μL/min/mg protein]	48/-	34/-	16/-	19/-	16/<10	14/<10
hepatocyte CLint (m/h) [μl/min/10^6 cells]	90.7/-	99.7/-	-/-	26.7/-	15.9/6.6	∼15/6.2
log *P*	2.10	1.90	2.10	1.85	2.25	2.34

Table 7. Overview of Subunit Specific *In Vitro* Biochemical IC_{50} Values of Compound 50[a]

Compound	Structure	β1i IC_{50} [nM]	β2i IC_{50} [nM]	β5i IC_{50} [nM]	β1 IC_{50} [nM]	β2 IC_{50} [nM]	β5 IC_{50} [nM]
50	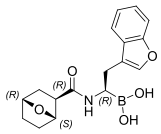	>30000	>30000	**3.6** ±2.4	>30000	>30000	2500 ±396

[a]Assay data represent the mean of a minimum of three determinations including the standard deviation if applicable.

mg/kg to U266B1 tumor-bearing mice (Figure 5). In this experiment, the single treatment of **50** at 1 mg/kg significantly reduced LMP7 activity compared to the vehicle control group for up to 14 h, with LMP7 activity returning to baseline by 24 h. Consistent with the PD effects described above for repeated application of **50** at 0.3 mg/kg, a single treatment at this same dose suppressed LMP7 activity at 1 and 6 h, yet it was without effects by 14 h. A higher dose of 1 mg/kg led to a dose-proportional increase in **50** exposure, which was associated with more prolonged suppression of tumor LMP7 activity.

https://doi.org/10.1021/acs.jmedchem.1c00604
J. Med. Chem. 2021, 64, 10230−10245

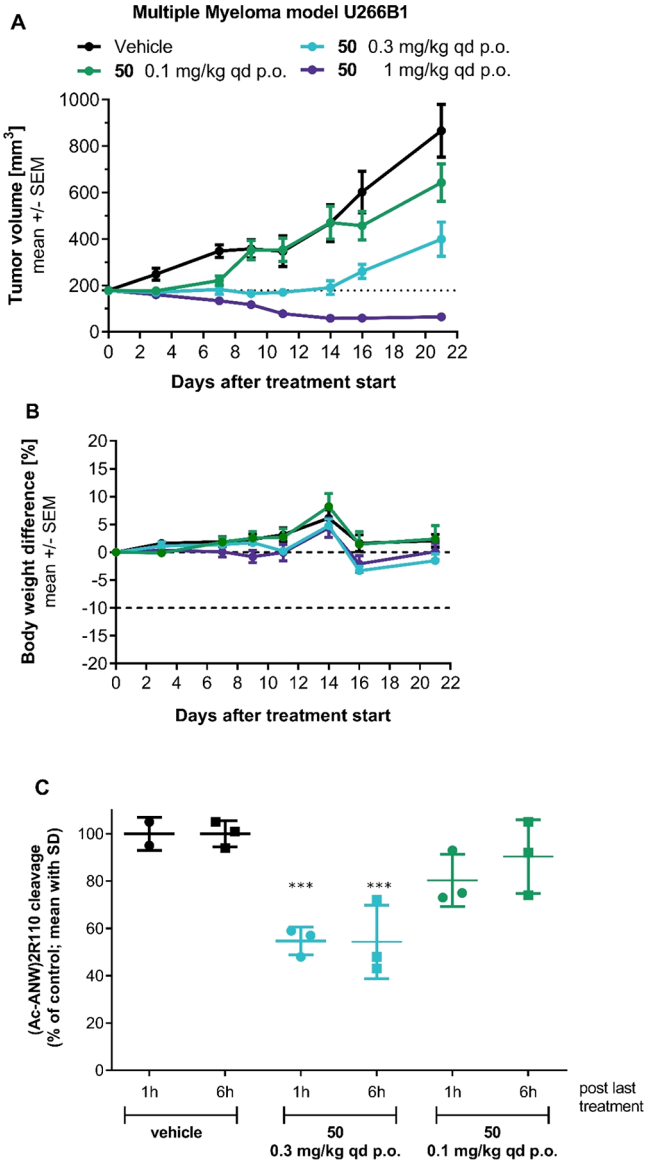

Figure 4. *In vivo* efficacy study with **50** in the MM model U266B1. (A) Tumor growth inhibition upon once daily oral treatment with 0.1, 0.3, and 1 mg/kg of **50**. (B) Body weight of U266B1 tumor-bearing mice treated with **50**. (C) LMP7 activity was determined in tumor lysates by employing the LMP7-specific fluorescent (Ac-ANW)2R110 cleavage assay at 1 and 6 h after the last treatment. Inhibition of LMP7 in treated samples was calculated relative to vehicle-treated tumors. ***$P < 0.001$.

Together, these data suggest that the elevated antitumor activity observed with the 1 mg/kg dose of **50**, compared to reduced dose levels, is likely explained by a longer duration of tumor LMP7 inhibition.

CONCLUSIONS

The iP subunit LMP7 has been implicated in the pathogenesis of diverse disease settings including autoimmunity, inflammation, and selected malignancies. However, up until very recently, pharmacological assessment of the role of LMP7 in preclinical models of these diseases has been hampered by the unavailability of LMP7 inhibitors exhibiting high target selectivity and DMPK and physicochemical properties enabling *in vivo* application. Our LMP7 inhibitor discovery program, based on rational drug design and structural insights, culminated in the identification of the highly potent and exquisitely selective amido boronic acid-based LMP7 inhibitor **50** (M3258).[41] The high potency and selectivity of M3258 were achieved via the combination of the amido boronic acid scaffold with a 3-benzo-furanyl moiety as the R_1 group. This allowed optimal interaction with the large and lipophilic S1 pocket of LMP7 while fitting less efficiently into other iP and cP proteolytic subunits. Furthermore, the (1*S*,2*R*,4*R*)-7-oxabicyclo[2.2.1]heptane-2-carboxylic amide R_2 group of M3258 is positioned such that the ether-oxygen forms a highly specific H-bond interaction with the peptide backbone of LMP7 but not with other iP or cP subunits.

The attractive overall profile of M3258 enabled its application in preclinical *in vivo* models of MM. These studies provided convincing preclinical evidence that LMP7 inhibition could be an attractive pharmacological strategy in this disease. Furthermore, our findings suggest that the spectrum of iP proteolytic subunit inhibition required to achieve efficacy in preclinical MM models contrasts starkly to that in models of autoimmunity and inflammation.[16−18] Similar to previous reports using other selective LMP7 inhibitors,[17,46] we have recently reported that M3258 was not cytotoxic toward diverse primary human cell types including PBMCs.[42] To our knowledge, the *in vivo* activity of these other LMP7 inhibitors in MM models has not yet been reported but would be of high interest for future studies to further understand the value of LMP7 inhibition in MM. In conclusion, the findings with M3258 reported here, and those from nonclinical safety studies (Sloot et al., manuscript in preparation), supported the recent initiation of a phase I clinical trial of M3258 in relapsed/refractory MM patients (ClinicalTrials.gov identifier: NCT04075721).

EXPERIMENTAL SECTION

Chemistry. *General Information.* All reactions were carried out under a nitrogen atmosphere or in sealed vials unless noted otherwise. Commercial reagents and dry solvents were used as purchased without additional purification. Reactions were magnetically stirred. Nuclear magnetic resonance (NMR) spectra were recorded on Bruker NMR Spectrometers operating at 400, 500, or 700 MHz for ^{1}H and 101 or 176 Hz for ^{13}C, respectively, and are referenced to tetramethyl silane as the internal standard. Compounds reported in the publication have a purity of >95% unless noted otherwise. NMR data were processed using MestreNova software and recorded as follows: ^{1}H NMR: chemical shift (δ, ppm), multiplicity (s, singlet; d, doublet; t, triplet; q, quartet; m, multiplet), coupling constant (Hz), and integration; ^{13}C NMR: chemical shift (δ, ppm). In the case of boronic acid samples, which usually contain varying ratios of monomer/trimer, D_2O was added to sharpen the NMR peaks. High-resolution mass spectra (HRMS) were recorded on a Bruker Daltonik maXis mass spectrometer. GC−MS spectra of boronic acids have been acquired after transformation into the corresponding boronic acid ethylene glycol esters using a Waters GCT Premier (ion source temperature: 230 °C, EI ionization at 70 eV). Thin-layer chromatography (TLC) was performed on Merck Silica gel 60 F254 plates and visualized with UV light.

LCMS Analysis. For monitoring of reactions and purity assessment, the following devices and methods have been used: UPLC-MS method: Waters Acquity UPLC; column CORTECS C18 (1.6 μm, 50−2.1 mm) flow: 0.9 mL/min, buffer A: H_2O + 0.05% HCOOH; buffer B: MeCN + 0.04% HCOOH; *T*: 40 °C, 0−1.0 min 2% → 100% B; 1.0−1.3 min 100% B. HPLC method: Elite La Chrom; column: Waters XBridge C8 (3.5 μm 50 × 4.6 mm); flow: 2 mL/min; 215 nm; buffer A: 0.05% TFA/H_2O; buffer B: 0.04% TFA/ACN; 0.0−0.2 min 5% buffer B; 0.2−8.1 min 5% → 100% buffer B; 8.1−

https://doi.org/10.1021/acs.jmedchem.1c00604
J. Med. Chem. 2021, 64, 10230−10245

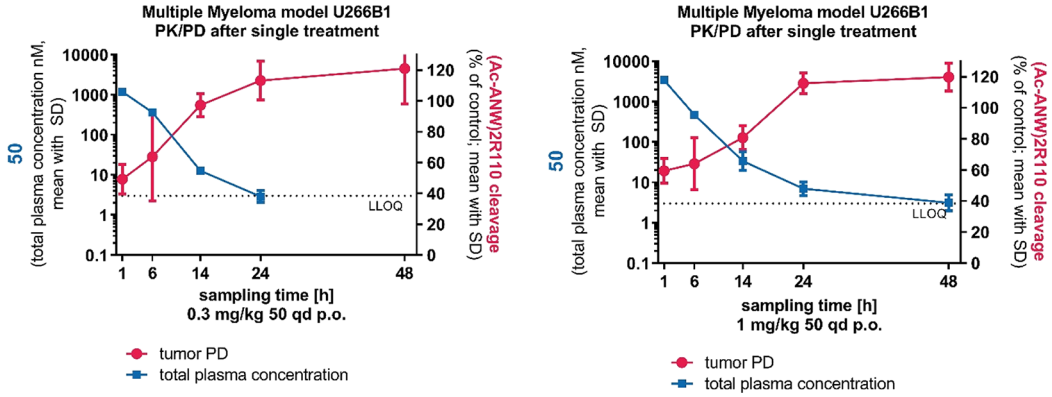

Figure 5. PK/PD correlation after treatment with 0.3 and 1.0 mg/kg qd p.o. **50**, respectively. Plasma samples were taken at 1, 6, 14, 24, and 48 h for PK analysis. LMP7 activity was determined in tumor lysates by employing the LMP7-specific fluorescent (Ac-ANW)2R110 cleavage assay. Inhibition of LMP7 in treated samples was calculated relative to vehicle-treated tumors. Total exposure of **50** in the plasma of mice was measured as described in the Experimental Section.

Scheme 4. Synthesis of α-Aminoboronic Acid Intermediate 58[a]

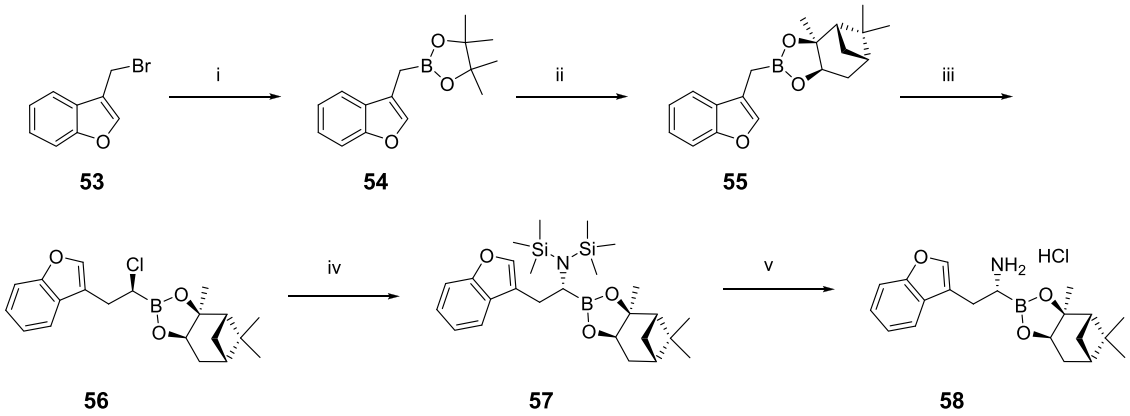

[a]Reagents and conditions: (i) B_2pin_2, $Pd(PPh_3)_4$, KOAc, dioxane, 85 °C, 16 h ; (ii) (+)-pinanediole, diethyl ether, room temperature, 16 h; (iii) Matteson homologation: (1) DCM, BuLi, −100 to −78 °C; (2) $ZnCl_2$, −78 °C to room temperature; (iv) LiHMDS, −78 °C to room temperature, 18 h; (v) HCl in ether, −10 °C to room temperature, 2 h.

Scheme 5. Synthesis of Intermediate 59 and of 50 (M3258)[a]

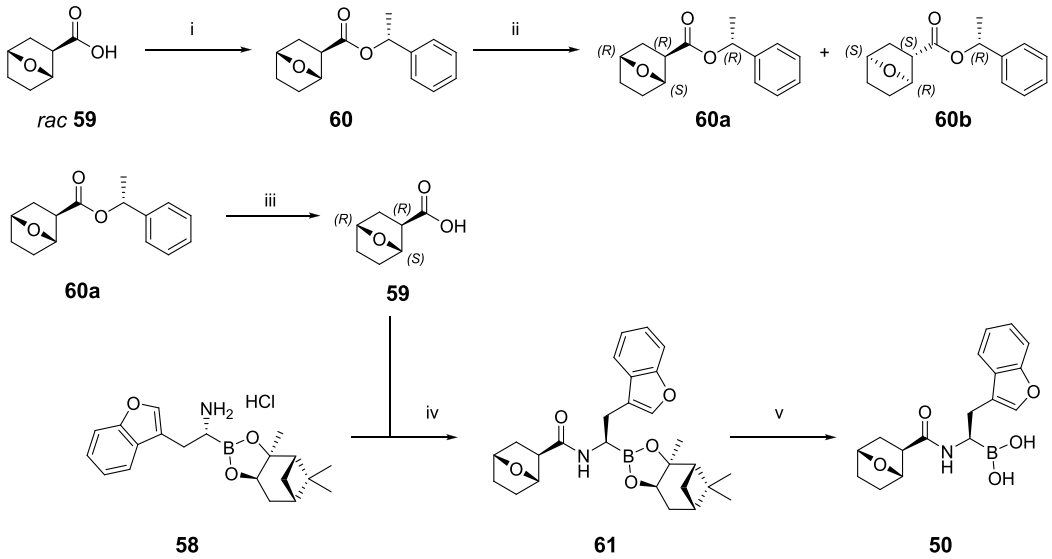

[a]Reagents and conditions: (i) (*R*)-1-phenylethanol, DMAP, EDCI, DCM, 0 °C; (ii) chiral separation; (iii) H_2, Pd/C, THF; (iv) **59**, HATU, DMF, DIPEA, room temperature, 2 h; (v) isobutylboronic acid, 2 N HCl, MeOH, pentane, room temperature, overnight.

https://doi.org/10.1021/acs.jmedchem.1c00604
J. Med. Chem. 2021, 64, 10230−10245

10.0 min 100% → 5% buffer B. Chromatography purifications were performed on a Teledyne Isco Combiflash system utilizing Redisept columns using a mobile phase composed of either ethyl acetate/heptane/ or dichloromethane/methanol.

The synthesis of **50** (M3258) is shown in Schemes 4 and 5. The synthesis of key intermediate **58** is exemplified as a typical procedure for the preparation of a protected α-amino-boronate building block. Preparation of **4**−**52** followed similar methods using commercial starting materials. The descriptions of general methods, characterizations, and spectra of all final compounds are available in the Supporting Information.

*2-(Benzofuran-3-ylmethyl)-4,4,5,5-tetramethyl-1,3,2-dioxaborolane (**54**).* To a solution of 3-(bromomethyl)benzofuran (7.1 g, 33.8 mmol) in degassed 1,4-dioxane (70 mL) were added bis(pinacolato)-diboron (10.3 g, 40.5 mmol), potassium carbonate (13.9 g, 101.0 mmol), and tetrakis(triphenylphosphine)palladium(0) (1.9 g, 1.7 mmol), and the mixture was stirred at 85 °C for 16 h. The reaction mixture was cooled to room temperature and filtered through a celite bed. The filtrate was concentrated, and the crude was purified by flash column chromatography on silica gel, eluting with 2−5% of ethyl acetate in petroleum ether to afford the title compound (6.1 g, 69%) as yellow oil. ^{1}H NMR (400 MHz, $CDCl_3$): δ 7.57−7.52 (m, 2H), 7.46−7.44 (m, 1H), 7.30−7.21 (m, 2H), 2.23 (s, 2H), 1.29 (s, 12H). ^{13}C NMR (101 MHz, DMSO): δ 154.4, 141.4, 128.7, 124.0, 122.1, 119.7, 116.1, 111.1, 83.3, 24.5, 5.6 HRMS: calcd for $C_{15}H_{19}BO_3$ M = 258.1427; found M = 258.1426.

*2-(Benzofuran-3-ylmethyl) Boronic Acid (+)-Pinanediol Ester (**55**).* To a solution of 2-(benzofuran-3-ylmethyl)-4,4,5,5-tetramethyl-1,3,2-dioxaborolane (6.1 g, 23.6 mmol) in diethyl ether (60 mL) was added (1*S*,2*S*,3*R*,5*S*)-(+)-pinanediol (6.0 g, 35.4 mmol), and the clear solution was stirred at room temperature for 12 h. The reaction mixture was washed twice with water and brine and dried over anhydrous sodium sulfate. The solvent was evaporated under vacuum, and the remaining oil was purified by flash column chromatography on silica gel, eluting with 5% of ethyl acetate in petroleum ether, to afford the title compound (6.3 g, 82%) as a solid. ^{1}H NMR (400 MHz, $CDCl_3$): δ 7.58−7.56 (m, 1H), 7.55−7.53 (m, 1H), 7.46−7.44 (m, 1H), 7.28−7.23 (m, 2H), 4.33 (dd, J = 1.88, 8.76 Hz, 1H), 2.34−2.32 (m, 1H), 2.28 (s, 2H), 2.22−2.21 (m, 1H), 2.08 (t, J = 5.88 Hz, 1H), 1.42 (s, 3H), 1.29 (s, 3H), 1.13 (d, J = 10.92 Hz, 1H), 0.85 (s, 3H). ^{13}C NMR (176 MHz, DMSO): δ 154.4, 141.4, 128.7, 124.0, 122.1, 119.8, 116.2, 111.1, 85.5, 77.0, 50.7, 38.9, 37.7, 35.0, 28.3, 26.8, 25.9, 23.6, 5.1. GCMS: m/z: 310. HRMS: calcd for $C_{19}H_{23}BO_3$: M = 310.1740; found M = 310.1752.

*[(1S)-1-Chloro-2-(benzofuran-3-ylmethyl)] Boronic Acid (+)-Pinanediol Ester (**56**).* To a cooled (−95 °C) mixture of dichloromethane (6.3 mL, 60.9 mmol) and anhydrous THF (36 mL) was added *n*-butyl lithium (1.6 M in hexanes, 14.0 mL, 22.3 mmol) over 20 min. After stirring for 20 min. at −95 °C, a solution of 2-(benzofuran-3-ylmethyl) boronic acid (+)-pinanediol ester (6.3 g, 20.3 mmol) in anhydrous THF (22 mL) was added over 20 min. Then, a solution of anhydrous zinc chloride (0.5 M in THF, 36.5 mL, 18.2 mmol) was added at −95 °C for 30 min while maintaining the inner temperature between −95 and − 100 °C. The mixture was allowed to reach room temperature and stirred for 18 h, and the solvent was removed under vacuum. To the resulting oil was added diethyl ether and saturated ammonium chloride. The organic layer was dried over anhydrous sodium sulfate and concentrated *in vacuo* (residue: 7.3 g, 99%). ^{1}H NMR (400 MHz, DMSO-d_6): δ 7.60−7.57 (m, 2H), 7.49−7.47 (m, 1H), 7.31−7.25 (m, 2H), 4.36−4.34 (m, 1H), 3.31−3.29 (m, 1H), 3.24−3.22 (m, 1H), 2.35−2.31 (m, 1H), 2.14−2.12 (m, 1H), 2.06 (t, J = 5.84 Hz, 1H), 1.90−1.86 (m, 2H), 1.42 (s, 3H), 1.04 (d, J = 11.04 Hz, 1H), 0.85 (s, 3H). ^{13}C NMR (176 MHz, DMSO): δ 154.4, 143.2, 127.3, 124.3, 122.4, 119.9, 116.8, 111.1, 86.1, 77.4, 50.6, 42.0, 38.6, 37.7, 34.6, 27.9, 27.8, 26.6, 25.4, 23.4. GCMS: m/z: 358.2. HRMS: calcd for $C_{20}H_{24}BClO_3$: 358.1507; found: 358.1501.

*[(1R)-1-[Bis(trimethylsilyl)amino]-2-(benzofuran-3-ylmethyl)] Boronic Acid (+)-Pinanediol Ester (**57**).* To a cooled (−78 °C) solution of [(1*S*)-1-chloro-2-(benzofuran-3-ylmethyl)]boronic acid (+)-pinanediol ester (7.3 g, 20.3 mmol) in 40 mL of anhydrous THF was added lithium bis(trimethylsilyl)amide (1 M in THF, 25.5 mL, 25.5 mmol). The mixture was allowed to reach room temperature, stirred for 18 h, and concentrated to dryness. To the resulting residue heptane was added, and then the precipitated solid was filtered off. The filtrate was concentrated to give the crude title compound (6.7 g, 68%). ^{1}H NMR (400 MHz, $CDCl_3$): δ 7.60−7.59 (m, 1H), 7.50−7.45 (m, 2H), 7.28−7.24 (m, 2H), 4.31 (dd, J = 1.56, 8.70 Hz, 1H), 3.18−3.14 (m, 1H), 2.92−2.90 (m, 1H), 2.75−2.72 (m, 1H), 2.34−2.30 (m, 1H), 2.15−2.14 (m, 1H), 2.03 (t, J = 5.68 Hz, 1H), 1.88−1.80 (m, 2H), 1.39 (s, 3H), 1.30 (s, 3H), 1.01 (d, J = 10.88 Hz, 1H), 0.84 (s, 3H), 0.09 (s, 18H).

*[(1R)-1-Amino-2-(Benzofuran-3-Ylmethyl)] Boronic Acid (+)-Pinanediol Ester Hydrochloride (**58**).* To a stirred, cooled (−10 °C) solution of [(1*R*)-1-[bis(trimethylsilyl)amino]-2-(benzofuran-3-ylmethyl)]boronic acid (+)-pinanediol ester (6.7 g, 13.9 mmol) in MTBE (30 mL) under nitrogen a solution of hydrochloride acid in ethyl acetate (2.50 eq.) was added dropwise. The reaction mixture was stirred at room temperature for 3 h, resulting in a precipitate. The reaction mixture was evaporated to dryness, and the obtained solid was triturated with MTBE and filtered. The filtered solid was washed with cold MTBE and dried under vacuum to afford the title compound (3.76 g, white solid, 72%). ^{1}H NMR (400 MHz, DMSO-d_6): δ 7.66 (s, 1H), 7.61−7.60 (m, 1H), 7.47−7.45 (m, 1H), 7.29−7.20 (m, 2H), 4.30−4.28 (m, 1H), 3.27−3.16 (m, 3H), 2.25−2.13 (m, 3H), 1.94 (t, J = 5.56 Hz, 1H), 1.86−1.81 (m, 2H), 1.25 (s, 6H), 1.01 (d, J = 8.00 Hz, 1H), 0.75 (s, 3H). ^{13}C NMR (126 MHz, DMSO-d_6): δ 154.6, 143.5, 127.3, 124.4, 122.5, 119.7, 115.1, 111.3, 86.8, 77.5, 50.5, 38.6, 37.7, 35.6, 34.4, 27.9, 26.7, 25.6, 23.5, 23.1. HRMS: calcd for $C_{20}H_{24}BNO_3$ $[M - 2H]^+$: 337.1849; found: 337.1849.

*(1S,2R,4R)-7-Oxa-bicyclo[2.2.1]heptane-2-carboxylic Acid (R)-1-Phenyl-ethyl Ester (**60a**).* To a solution of *rac* 7-oxa-bicyclo[2.2.1]-heptane-2-carboxylic acid (4.68 g; 31.3 mmol, racemic) in dry dichloromethane (100 mL) under an atmosphere of argon (*R*)-1-phenyl-ethanol (4.62 mL; 37.5 mmol), 4-(dimethylamino)pyridine for synthesis (DMAP) (3.82 g; 31.3 mmol), and (3-dimethylamino-propyl)-ethyl-carbodiimide hydrochloride (EDCI) (6.73 g; 34.4 mmol) were added under stirring at 0 °C. Subsequently, the clear reaction solution was stirred overnight at room temperature. After completion of the ester formation, the reaction was quenched by adding sat. NH_4Cl(aq) solution and the mixture was extracted twice with CH_2Cl_2. The organic layer was washed thrice with sat. $NaHCO_3$(aq) and brine, dried over Na_2SO_4, filtrated, and evaporated to dryness. The crude product was purified by flash chromatography (silica gel; *n*-heptane/ethyl acetate, 0−30% ethyl acetate) to obtain 7.50 g (30.4 mmol, yield: 97.3%) of a colorless oil (HPLC: 100% pure, mixture of diastereomers). The mixture of diastereomers was separated by preparative, chiral HPLC (Chiralcel OD-H; *n*-heptane/2-propanol, 95/5; 220 nm) to obtain (1*R*,2*S*,4*S*)-7-oxa-bicyclo[2.2.1]-heptane-2-carboxylic acid (*R*)-1-phenyl-ethyl ester (3.22 g, colorless oil, yield: 41.8%, chiral HPLC 100%) and (1*S*,2*R*,4*R*)-7-oxa-bicyclo[2.2.1]heptane-2-carboxylic acid (*R*)-1-phenyl-ethyl ester (3.14 g, oil, yield: 40.7%, chiral HPLC 100%). HRMS: calcd for $C_{15}H_{18}O_3$: 246.1256; found: 246.1256.

*(1S,2R,4R)-7-Oxabicyclo[2.2.1]heptane-2-carboxylic Acid (**59**).* To a solution of (1*S*,2*R*,4*R*)-7-oxa-bicyclo[2.2.1]heptane-2-carboxylic acid (*R*)-1-phenyl-ethyl ester (46.74 g; 182.75 mmol; 1.00 equiv) in THF (233.70 mL), palladium on carbon (10% w/w) (1.94 g; 1.83 mmol; 0.01 equiv) was added. The reaction mixture is hydrogenated under a H_2 atmosphere at 50 °C and 5 bar pressure for 16 h. After completion of the hydrogenation, the reaction mixture was filtered through celite, and the filtrate was evaporated to dryness and taken up in pentane. The organic layer was extracted thrice with water. Subsequently, the water layer was lyophilized to obtain (1*S*,2*R*,4*R*)-7-oxabicyclo[2.2.1]heptane-2-carboxylic acid (22.62 g; 159.1 mmol; yield: 87.1%) as a colorless solid. TLC: chloroform/methanol (9.5/0.5), R_f: 0.5. ^{1}H NMR 400 MHz, DMSO-d_6: 12.16 (s, 1H), 4.66 (d, J = 4.4 Hz, 1H), 4.54 (t, J = 4.4 Hz, 1H), 2.57 (d, J = 35.2 Hz, 1H), 1.91−1.86 (m, 1H), 1.65−1.37 (m, 4H), 1.34−1.33 (m, 1H). HRMS

https://doi.org/10.1021/acs.jmedchem.1c00604
J. Med. Chem. 2021, 64, 10230−10245

calcd for $C_7H_{10}O_3$: 142.0630; found: 142.0629. Optical rotation: $[\alpha]_D^{20}$ = + 31.9° (ethanol, 20.16 mg/10 mL).

*(1S,2R,4R)-7-Oxa-bicyclo[2.2.1]heptane-2-carboxylic Acid [(R)-2-(Benzofuran-3-yl)-1-((1S,2S,6R,8S)-2,9,9-trimethyl-3,5-dioxa-4-bora-tricyclo[6.1.1.0^{2,6}]dec-4-yl)-ethyl]-amide (**61**).* To a solution of (1*S*,2*R*,4*R*)-7-oxa-bicyclo[2.2.1]heptane-2-carboxylic acid (1.87 g; 13.18 mmol), HATU (4.62 g; 14.37 mmol), and 4-methylmorpholine (3.29 mL; 29.94 mmol) in 70 mL of dry DMF was added under ice cooling and an argon atmosphere (*R*)-2-(benzofuran-3-yl)-1-((1*S*,2*S*,6*R*,8*S*)-2,9,9-trimethyl-3,5-dioxa-4-boratricyclo-[6.1.1.0^{2,6}]dec-4-yl)-ethylamine hydrochloride (4.50 g; 11.98 mmol). The yellow solution was stirred for 2.5 h at room temperature. The reaction mixture was poured into 500 mL of ice-cooled, saturated $NaHCO_3$ solution and stirred for 15 min to give a precipitate, which was collected by vacuum filtration and washed with water. The obtained solid was triturated with acetonitrile, diluted with MTB-ether, and sucked off to yield (1*S*,2*R*,4*R*)-7-oxa-bicyclo[2.2.1]-heptane-2-carboxylic acid [(*R*)-2-(benzofuran-3-yl)-1-((1*S*,2*S*,6*R*,8*S*)-2,9,9-trimethyl-3,5-dioxa-4-bora-tricyclo[6.1.1.0^{2,6}]dec-4-yl)-ethyl]-amide (3.26 g, yield: 58.8%) as white solid (purity: 100%). ^{1}H NMR (700 MHz, DMSO-d_6): δ 9.23−9.21 (m, 1H), 7.74−7.73 (m, 1H), 7.58−7.56 (m, 1H), 7.54−7.52 (m, 1H), 7.30−7.27 (m, 1H), 7.26−7.23 (m, 1H), 4.60−4.57 (m, 2H), 4.00 (dd, *J* = 8.6, 2.3 Hz, 1H), 2.82−2.78 (m, 1H), 2.78−2.75 (m, 1H), 2.71 (dd, *J* = 9.1, 5.0 Hz, 1H), 2.66−2.62 (m, 1H), 2.17−2.12 (m, 1H), 1.91−1.86 (m, 1H), 1.84−1.80 (m, 1H), 1.77 (t, *J* = 5.6 Hz, 1H), 1.73−1.69 (m, 2H), 1.61−1.58 (m, 1H), 1.58−1.51 (m, 2H), 1.51−1.47 (m, 1H), 1.45−1.42 (m, 1H), 1.26 (d, *J* = 9.9 Hz, 1H), 1.20 (s, 3H), 1.19 (s, 3H), 0.79 (s, 3H). ^{13}C NMR (176 MHz, DMSO-d_6): δ 177.8, 154.5, 142.4, 128.1, 123.9, 122.2, 119.6, 118.3, 111.1, 81.8, 78.2, 75.3, 75.2, 52.0, 44.3, 41.7, 39.9, 37.5, 36.4, 34.1, 29.3, 29.2, 28.6, 27.1, 25.8, 25.1, 23.9. LCMS method A: (M + H) 464.2; Rt: 2.57 min.

*[(1R)-2-(1-Benzofuran-3-yl)-1-{[(1S,2R,4R)-7-oxabicyclo[2.2.1]-heptan-2-yl]formamido} ethyl]boronic Acid (**50**).* To a two-phase system of (1*S*,2*R*,4*R*)-7-oxa-bicyclo[2.2.1]heptane-2-carboxylic acid [(*R*)-2-benzofuran-3-yl-1-((1*S*,2*S*,6*R*,8*S*)-2,9,9-trimethyl-3,5-dioxa-4-bora-tricyclo[6.1.1.0^{2,6}]dec-4-yl)-ethyl]-amide (ee = 97%, 3.45 mmol; 1.60 g) in 150 mL of *n*-pentane and 50 mL methanol were added isobutylboronic acid (13.81 mmol; 1.41 g) and 1 N hydrochloric acid (15.54 mmol; 15.54 mL) at 0 °C. The reaction was stirred at room temperature overnight. The pentane phase was discarded, and the methanolic phase was washed with pentane (3×, 80 mL). The methanolic phase was concentrated (bath temp. below 30 °C) *in vacuo*, diluted with ice water, and alkalized with 1 N NaOH (pH 11−12). This basic solution was extracted with DCM (3 × 80 mL). The aqueous phase was acidified with 1 N HCl (pH 2) and extracted with DCM (5 × 80 mL) again. The combined organic phase was dried over Na_2SO_4, filtrated, and evaporated. The residue was dissolved in acetonitrile/water and lyophilized to give 0.697 g (yield: 61.3%) of the title compound as white powder. ^{1}H NMR (500 MHz, DMSO-d_6/D_2O): δ 7.61 (s, 1H), 7.59 (d, *J* = 7.7 Hz, 1H), 7.48 (d, *J* = 8.1 Hz, 1H), 7.29−7.25 (m, 1H), 7.24−7.19 (m, 1H), 4.48−4.45 (m, 1H), 4.42−4.40 (m, 1H), 3.12−3.08 (m, 1H), 2.84 (dd, *J* = 14.9, 5.9 Hz, 1H), 2.73 (dd, *J* = 14.9, 8.3 Hz, 1H), 2.45 (dd, *J* = 9.1, 4.9 Hz, 1H), 1.76−1.71 (m, 1H), 1.60 (dd, *J* = 11.9, 9.1 Hz, 1H), 1.52−1.44 (m, 2H), 1.43−1.34 (m, 2H). ^{13}C NMR (176 MHz, DMSO-d_6): δ 174.6, 155.0, 142.6, 128.6, 124.7, 122.9, 120.4, 118.9, 111.7, 79.4, 75.9, 47.7, 40.7, 34.8, 29.8, 29.3, 24.9. GC−MS: calcd as ethylene glycol ester $C_{19}H_{22}BNO_5$ M = 355.1591; found: 355.1568.

Biological Assays. *Biochemical Activity Testing.* Human immunoproteasomes, purified as described previously[47] and used at 0.25 nmol/L, or purified human constitutive proteasomes (Boston Biochem, used at 1.25 nmol/L) were preincubated for 2 h at 25 °C in 384-well plates with compounds or the vehicle dimethyl sulfoxide (DMSO) in an assay buffer containing 20 mmol/L Tris (pH 7.5), 0.03% sodium dodecyl sulfate (SDS), and 1 mmol/L ethylenediaminetetraacetic acid (EDTA). The following fluorogenic peptidic substrates (from Bachem Holding, unless stated otherwise), which undergo preferential processing by specific proteasome subunits, were added at the indicated final concentrations to assess the inhibitory activity of compounds: Ac-nLPnLD-AMC at 50 μmol/L for β1, (Ac-PAL)2R110 (Biomol) at 80 μmol/L for LMP2, Ac-RLR-AMC at 20 μmol/L for β2 and MECL-1, and Suc-LLVY-AMC at either 40 μmol/L for LMP7 or at 50 μmol/L for β5.[30] Fluorescence was measured using an Envision 2104 plate reader (PerkinElmer) immediately following substrate addition and again after 1 h of incubation. Excitation and emission settings were used in accordance with the instructions of the provider of each peptide substrate. The inhibitory activity of compounds was ascertained by calculating the difference in fluorescence at each time point. IC_{50} values for each compound were calculated by nonlinear regression analysis, normalized to DMSO controls, using Genedata Screener (Genedata).

Cellular Assays. Like in the biochemical assays, the cellular potencies of compounds were determined by measuring the proteolytic activities of proteasome subunits toward specific substrates. PBMCs (AccuCell Human PBMC) were used to assess the activity of cellular LMP7 (β5i). A549 cells (ATCC no. CRL-185) were used to assess cellular β5 activity. A549 cells have previously been shown to dominantly express the cP.[48] Both cell lines were applied at a final concentration of 3 × 10^5 cells/ml. The assays were conducted in tissue culture plates (384 wells, white, PS) from Greiner. Compound dilution series were prepared in DMSO. The frozen cells were diluted to a stock concentration of 4.5 × 10^5 cells/ml in DMEM/10% FCS. Cell suspension (22.5 μL) was added in each well of the test plate. After an incubation (2 h, 5% CO_2), 50 nL of compound solution or vehicle (DMSO) was added to each well. After shaking for 15 s at 900 rpm, the plates were incubated for 2 h at 7 °C (5% CO_2). Then, 12.5 μL of Proteasome-Glo detection solution was then added (prepared according to the manufacturer's instructions). For the cellular LMP7 (β5i) assay, the Proteasome-Glo custom kit from Promega (Ac-ANW-luciferin substrate) was used. For the β5 assay, the Proteasome-Glo Chymotrypsin-Like Cell-Based Assay kit from Promega (Suc-LLVY-luciferin substrate) was used. After shaking for 15 s at 900 rpm and 30 min of incubation at room temperature, a luminometric readout was performed. These data served as the basis for the calculation of IC_{50} values as described above for the biochemical assays.

Efficacy Testing In Vivo (All Animal Experiments Performed in the Manuscript were Conducted in Compliance with Institutional Guidelines). The human MM cell line U266B1 was obtained from ATCC (TIB-196). A suspension (100 μL) of 5 million cells in phosphate-buffered saline (PBS) mixed with 1:1 Matrigel (Becton Dickinson) was subcutaneously injected into H2d Rag2 female mice. Once tumors reached a mean tumor volume of 179 mm^3, animals were assigned to treatment groups (*n* = 10) and compound **50** was administered at doses of 0.1, 0.3, and 1 mg/kg daily *per os* (formulation: 0.5% Methocel Premium K4M (Colorcon) and 0.25% Tween 20 in PBS). Mean tumor volume and standard error of the mean (SEM) were measured. Statistical analyses were performed using repeated measures analysis of covariance.

In Vivo PD. For PD analyses of xenograft tumors, 50−100 mg of tissue was lysed, and lysates were incubated with 10 μM LMP7 substrate (Ac-ANW)2R110 (Biomol) for 60 min at 37 °C. Fluorescence (excitation: 485 nm, emission: 535 nm) was measured, and percent of LMP7 inhibition was calculated relative to vehicle-treated controls.

In Vivo PK. For plasma sampling, blood was collected from mice via an axillary cut and transferred into tubes containing sodium heparin as the anticoagulant, mixed well, and then centrifuged at 12,000*g* for 3 min in a refrigerated centrifuge at 4 °C. Plasma was collected and transferred into Eppendorf tubes. Samples were stabilized by the addition of 1 μL of 22% formic acid per 10 μL of plasma and briefly mixed. The samples were stored on ice and protected from light before freezing at −20 °C until further PK analysis by UPLC-MS/MS.

X-ray Crystallography. A previously described method was used for the purification of human immunoproteasomes[47] using the following modifications. Ion exchange chromatography on a DAE-650 M and CHT ceramic hydroxyapatite was done to isolate immunoproteasomes. Ammonium sulfate was then added to the pooled fractions to a final concentration of 1.7 mol/L. Chromatog-

https://doi.org/10.1021/acs.jmedchem.1c00604
J. Med. Chem. 2021, 64, 10230−10245

raphy was then performed on Butyl-Sepharose followed by purification using a Superdex200 16/60 gel filtration column equilibrated in 50 mmol/L 4-(2-hydroxyethyl)-1-piperazineethanesulfonic acid (HEPES) (pH 7.6), 100 mmol/L NaCl and 1 mmol/L dithiothreitol (DTT). For crystallization trials, fractions containing the human immunoproteasomes were concentrated to 8−10 mg/mL by ultrafiltration and stored at −80 °C. Fractions obtained at each chromatographic step were tested for proteolytic activity using the immunoproteasome peptidic substrate cleavage assays described above, and enzymatically active fractions were pooled. Hanging-drop vapor diffusion from a 1:0.5 mixture of protein (6 mg/mL immunoproteasomes in 50 mmol/L HEPES (pH 7.6), 100 mmol/L NaCl, and 1 mmol/L DTT) and reservoir solution (0.2 mol/L sodium thiocyanate, 32−41% 2,4-methyl-pentanediol) was used to grow human immunoproteasome crystals. The quality of crystals was improved using cyclic temperature gradients between 15 and 18 °C. The immunoproteasome−cocrystal complex was formed by soaking immunoproteasome apo crystals in 10 mmol/L compound **4**. The immunoproteasome apo structure was solved by molecular replacement using Phaser (CCP4)[49] using the bovine constitutive proteasome as a starting model.[50] The structure of the immunoproteasome−cocrystal complex was subsequently solved by molecular replacement using the structure of apo immunoproteasome. COOT[51] was used for model building. REFMAC5 (CCP4) and BUSTER[52] were used for refinement.

■ ASSOCIATED CONTENT

Supporting Information

The Supporting Information is available free of charge at https://pubs.acs.org/doi/10.1021/acs.jmedchem.1c00604.

General procedures for compound preparation; characterization of all final products by ^{1}H NMR, ^{13}C NMR, HRMS, and HPLC; data collection and refinement statistics for the cocrystal structure of compound **4** in complex with the human 20S iP; extended biochemical profiling; and *in vitro* safety profiling (PDF)

Molecular formula strings (CSV)

■ AUTHOR INFORMATION

Corresponding Author

Markus Klein − *Merck KGaA, Darmstadt 64293, Germany;* orcid.org/0000-0003-3675-2637; Phone: +49 6151 727472; Email: markus.b.klein@merckgroup.com

Authors

Michael Busch − *Merck KGaA, Darmstadt 64293, Germany*

Manja Friese-Hamim − *Merck KGaA, Darmstadt 64293, Germany*

Stefano Crosignani − *Merck KGaA, Darmstadt 64293, Germany*

Thomas Fuchss − *Merck KGaA, Darmstadt 64293, Germany*

Djordje Musil − *Merck KGaA, Darmstadt 64293, Germany*

Felix Rohdich − *Merck KGaA, Darmstadt 64293, Germany*

Michael P. Sanderson − *Merck KGaA, Darmstadt 64293, Germany*

Jeyaprakashnarayanan Seenisamy − *Syngene International Limited, Bangalore 560 099, India*

Gina Walter-Bausch − *Merck KGaA, Darmstadt 64293, Germany*

Ugo Zanelli − *Merck KGaA, Darmstadt 64293, Germany*

Philip Hewitt − *Merck KGaA, Darmstadt 64293, Germany*

Christina Esdar − *Merck KGaA, Darmstadt 64293, Germany*

Oliver Schadt − *Merck KGaA, Darmstadt 64293, Germany*

Complete contact information is available at: https://pubs.acs.org/10.1021/acs.jmedchem.1c00604

Author Contributions

The manuscript was written by M.K., O.S., and M.P.S. with contributions from all authors. All authors approved the manuscript.

Notes

The authors declare no competing financial interest.

■ ACKNOWLEDGMENTS

We acknowledge the support and contributions of the following people: Andreas Becker, Andrée Blaukat, Julie DeMartino, Hugues Dolgos, Elise Drouin, Samer El Bawab, Ralf Emmerich, Stefanie Gaus, Claude Gimmi, Samantha Goodstal, Philipp Haselmayer, Hendrik Hollmann, Frank Jährling, Dilafruz Juraeva, Mirek Jurzak, Mireille Krier, Daniel Kuhn, Long Li, Floriane Lignet, Laura Liu, Jianguo Ma, Pia Sanfelice, Melanie Schwarz, Willem Sloot, Sofia Stinchi, Heinz Thoma, Klaus Urbahns, Anja Victor, Ping Yu, and Lars zur Brügge. We also acknowledge the contribution of Proteros Biostructures GmbH (Germany), Lead Discovery Center GmbH (Germany), Pharmaron Beijing Co., Ltd. (China), and Syngene International Ltd. (India). The authors would like to thank Claudia Mahr, Heike Naumann, Andrea C. Delp, and Simone Jost for their synthesis support and generation of analytical data.

■ ABBREVIATIONS

cP,, constitutive proteasome; ER, efflux ratio; iP, immunoproteasome; IFNγ, interferon γ; LLOQ, lower limit of quantification; LMP2, low-molecular-mass polypeptide-2; MECL-1, multicatalytic endopeptidase complex-like 1; LMP7, low-molecular-mass polypeptide-7; MTBE, methyl *tert*-butyl ether; HATU, 1-[bis(dimethylamino)-methylene]-1*H*-1,2,3-triazolo[4,5-*b*]pyridinium 3-oxide hexafluorophosphate; PBMC, peripheral blood mononuclear cell; PD, pharmacodynamic; PK, pharmacokinetic; SAR, structure activity relationship; THF, tetrahydrofuran; TNFα, tumor necrosis factor α

■ REFERENCES

(1) Micale, N.; Scarbaci, K.; Troiano, V.; Ettari, R.; Grasso, S.; Zappalà, M. Peptide-based proteasome inhibitors in anticancer drug design. *Med. Res. Rev.* **2014**, *34*, 1001−1069.

(2) Groettrup, M.; Kirk, C. J.; Basler, M. Proteasomes in immune cells: more than peptide producers? *Nat. Rev. Immunol.* **2010**, *10*, 73−78.

(3) Miller, Z.; Lee, W.; Kim, K. B. The immunoproteasome as a therapeutic target for hematological malignancies. *Curr. Cancer Drug Targets* **2014**, *14*, 537−548.

(4) Altun, M.; Galardy, P. J.; Shringarpure, R.; Hideshima, T.; LeBlanc, R.; Anderson, K. C.; Ploegh, H. L.; Kessler, B. M. Effects of PS-341 on the activity and composition of proteasomes in multiple myeloma cells. *Cancer Res.* **2005**, *65*, 7896−7901.

(5) Eleuteri, A. M.; Angeletti, M.; Lupidi, G.; Tacconi, R.; Bini, L.; Fioretti, E. Isolation and characterization of bovine thymus multicatalytic proteinase complex. *Protein Expression Purif.* **2000**, *18*, 160−168.

(6) Noda, C.; Tanahashi, N.; Shimbara, N.; Hendil, K. B.; Tanaka, K. Tissue distribution of constitutive proteasomes, immunoproteasomes, and PA28 in rats. *Biochem. Biophys. Res. Commun.* **2000**, *277*, 348−354.

(7) Singh, A. V.; Bandi, M.; Aujay, M. A.; Kirk, C. J.; Hark, D. E.; Raje, N.; Chauhan, D.; Anderson, K. C. PR-924, a selective inhibitor of the immunoproteasome subunit LMP-7, blocks multiple myeloma cell growth both in vitro and in vivo. *Br. J. Haematol.* **2011**, *152*, 155−163.

(8) Hallermalm, K.; Seki, K.; Wei, C.; Castelli, C.; Rivoltini, L.; Kiessling, R.; Levitskaya, J. Tumor necrosis factor-alpha induces coordinated changes in major histocompatibility class I presentation pathway, resulting in increased stability of class I complexes at the cell surface. *Blood* **2001**, *98*, 1108−1115.
(9) Angeles, A.; Fung, G.; Luo, H. Immune and non-immune functions of the immunoproteasome. *Front. Biosci.* **2012**, *17*, 1904−1916.
(10) Kubiczkova, L.; Pour, L.; Sedlarikova, L.; Hajek, R.; Sevcikova, S. Proteasome inhibitors - molecular basis and current perspectives in multiple myeloma. *J. Cell. Mol. Med.* **2014**, *18*, 947−961.
(11) Cengiz Seval, G.; Beksac, M. The safety of bortezomib for the treatment of multiple myeloma. *Expert Opin. Drug Saf.* **2018**, *17*, 953−962.
(12) Ettari, R.; Zappalà, M.; Grasso, S.; Musolino, C.; Innao, V.; Allegra, A. Immunoproteasome-selective and non-selective inhibitors: a promising approach for the treatment of multiple myeloma. *Pharmacol. Ther.* **2018**, *182*, 176−192.
(13) Kuhn, D. J.; Orlowski, R. Z. The immunoproteasome as a target in hematologic malignancies. *Semin. Hematol.* **2012**, *49*, 258−262.
(14) Schlafer, D.; Shah, K. S.; Panjic, E. H.; Lonial, S. Safety of proteasome inhibitors for treatment of multiple myeloma. *Expert Opin. Drug Saf.* **2017**, *16*, 167−183.
(15) Basler, M.; Groettrup, M. Recent insights how combined inhibition of immuno/proteasome subunits enables therapeutic efficacy. *Genes Immun.* **2020**, *21*, 273−287.
(16) Basler, M.; Lindstrom, M. M.; LaStant, J. J.; Bradshaw, J. M.; Owens, T. D.; Schmidt, C.; Maurits, E.; Tsu, C.; Overkleeft, H. S.; Kirk, C. J.; Langrish, C. L.; Groettrup, M. Co-inhibition of immunoproteasome subunits LMP2 and LMP7 is required to block autoimmunity. *EMBO Rep.* **2018**, *19*, No. e46512.
(17) Ladi, E.; Everett, C.; Stivala, C. E.; Daniels, B. E.; Durk, M. R.; Harris, S. F.; Huestis, M. P.; Purkey, H. E.; Staben, S. T.; Augustin, M.; Blaesse, M.; Steinbacher, S.; Eidenschenk, C.; Pappu, R.; Siu, M. Design and evaluation of highly selective human immunoproteasome inhibitors reveal a compensatory process that preserves immune cell viability. *J. Med. Chem.* **2019**, *62*, 7032−7041.
(18) Johnson, H. W. B.; Lowe, E.; Anderl, J. L.; Fan, A.; Muchamuel, T.; Bowers, S.; Moebius, D. C.; Kirk, C.; McMinn, D. L. Required immunoproteasome subunit inhibition profile for anti-inflammatory efficacy and clinical candidate KZR-616 ((2 S,3 R)- N-((S)-3-(Cyclopent-1-en-1-yl)-1-((R)-2-methyloxiran-2-yl)-1-oxopropan-2-yl)-3-hydroxy-3-(4-methoxyphenyl)-2-((S)-2-(2-morpholinoacetamido)propanamido)propenamide). *J. Med. Chem.* **2018**, *61*, 11127−11143.
(19) Downey-Kopyscinski, S.; Daily, E. W.; Gautier, M.; Bhatt, A.; Florea, B. I.; Mitsiades, C. S.; Richardson, P. G.; Driessen, C.; Overkleeft, H. S.; Kisselev, A. F. An inhibitor of proteasome β2 sites sensitizes myeloma cells to immunoproteasome inhibitors. *Blood Adv.* **2018**, *2*, 2443−2451.
(20) Ettari, R.; Pallio, G.; Pizzino, G.; Irrera, N.; Zappalà, M.; Maiorana, S.; Di Chio, C.; Altavilla, D.; Squadrito, F.; Bitto, A. Non-covalent immunoproteasome inhibitors induce cell cycle arrest in multiple myeloma MM.1R cells. *J. Enzyme Inhib. Med. Chem.* **2019**, *34*, 1307−1313.
(21) Koerner, J.; Brunner, T.; Groettrup, M. Inhibition and deficiency of the immunoproteasome subunit LMP7 suppress the development and progression of colorectal carcinoma in mice. *Oncotarget* **2017**, *8*, 50873−50888.
(22) Niewerth, D.; Franke, N. E.; Jansen, G.; Assaraf, Y. G.; van Meerloo, J.; Kirk, C. J.; Degenhardt, J.; Anderl, J.; Schimmer, A. D.; Zweegman, S.; de Haas, V.; Horton, T. M.; Kaspers, G. J. L.; Cloos, J. Higher ratio immune versus constitutive proteasome level as novel indicator of sensitivity of pediatric acute leukemia cells to proteasome inhibitors. *Haematologica* **2013**, *98*, 1896−1904.
(23) Niewerth, D.; Kaspers, G. J.; Assaraf, Y. G.; van Meerloo, J.; Kirk, C. J.; Anderl, J.; Blank, J. L.; van de Ven, P. M.; Zweegman, S.; Jansen, G.; Cloos, J. Interferon-γ-induced upregulation of immunoproteasome subunit assembly overcomes bortezomib resistance in human hematological cell lines. *J. Hematol. Oncol.* **2014**, *7*, 7.
(24) Singh, P. K.; Fan, H.; Jiang, X.; Shi, L.; Nathan, C. F.; Lin, G. Immunoproteasome β5i-selective dipeptidomimetic inhibitors. *ChemMedChem* **2016**, *11*, 2127−2131.
(25) Yeo, I. J.; Lee, M. J.; Baek, A.; Miller, Z.; Bhattarai, D.; Baek, Y. M.; Jeong, H. J.; Kim, Y. K.; Kim, D. E.; Hong, J. T.; Kim, K. B. A dual inhibitor of the proteasome catalytic subunits LMP2 and Y attenuates disease progression in mouse models of Alzheimer's disease. *Sci. Rep.* **2019**, *9*, 18393.
(26) Demo, S. D.; Kirk, C. J.; Aujay, M. A.; Buchholz, T. J.; Dajee, M.; Ho, M. N.; Jiang, J.; Laidig, G. J.; Lewis, E. R.; Parlati, F.; Shenk, K. D.; Smyth, M. S.; Sun, C. M.; Vallone, M. K.; Woo, T. M.; Molineaux, C. J.; Bennett, M. K. Antitumor activity of PR-171, a novel irreversible inhibitor of the proteasome. *Cancer Res.* **2007**, *67*, 6383−6391.
(27) Dubiella, C.; Baur, R.; Cui, H.; Huber, E. M.; Groll, M. Selective inhibition of the immunoproteasome by structure-based targeting of a non-catalytic cysteine. *Angew. Chem., Int. Ed.* **2015**, *54*, 15888−15891.
(28) Kisselev, A. F.; van der Linden, W. A.; Overkleeft, H. S. Proteasome inhibitors: an expanding army attacking a unique target. *Chem. Biol.* **2012**, *19*, 99−115.
(29) Huber, E. M.; Heinemeyer, W.; de Bruin, G.; Overkleeft, H. S.; Groll, M. A humanized yeast proteasome identifies unique binding modes of inhibitors for the immunosubunit β5i. *EMBO J* **2016**, *35*, 2602−2613.
(30) Blackburn, C.; Gigstad, K. M.; Hales, P.; Garcia, K.; Jones, M.; Bruzzese, F. J.; Barrett, C.; Liu, J. X.; Soucy, T. A.; Sappal, D. S.; Bump, N.; Olhava, E. J.; Fleming, P.; Dick, L. R.; Tsu, C.; Sintchak, M. D.; Blank, J. L. Characterization of a new series of non-covalent proteasome inhibitors with exquisite potency and selectivity for the 20S β5-subunit. *Biochem. J.* **2010**, *430*, 461−476.
(31) Santos, R. d. L. A.; Bai, L.; Singh, P. K.; Murakami, N.; Fan, H.; Zhan, W.; Zhu, Y.; Jiang, X.; Zhang, K.; Assker, J. P.; Nathan, C. F.; Li, H.; Azzi, J.; Lin, G. Structure of human immunoproteasome with a reversible and noncompetitive inhibitor that selectively inhibits activated lymphocytes. *Nat. Commun.* **2017**, *8*, 1692.
(32) Zhu, Y.; Zhao, X.; Zhu, X.; Wu, G.; Li, Y.; Ma, Y.; Yuan, Y.; Yang, J.; Hu, Y.; Ai, L.; Gao, Q. Design, synthesis, biological evaluation, and structure-activity relationship (SAR) discussion of dipeptidyl boronate proteasome inhibitors, part I: comprehensive understanding of the SAR of alpha-amino acid boronates. *J. Med. Chem.* **2009**, *52*, 4192−4199.
(33) Groll, M.; Berkers, C. R.; Ploegh, H. L.; Ovaa, H. Crystal structure of the boronic acid-based proteasome inhibitor bortezomib in complex with the yeast 20S proteasome. *Structure* **2006**, *14*, 451−456.
(34) Klein, M.; Schadt, O.; Haselmayer, P.; Busch, M. Boronic acid derivatives. WO2,016,050,356. 2016.
(35) Ishiyama, T.; Murata, M.; Miyaura, N. Palladium(0)-catalyzed cross-coupling reaction of alkoxydiboron with haloarenes: a direct procedure for arylboronic esters. *J. Org. Chem.* **1995**, *60*, 7508−7510.
(36) Matteson, D. S.; Sadhu, K. M.; Lienhard, G. E. R-1-Acetamido-2-phenylethaneboronic acid. A specific transition-state analog for chymotrypsin. *J. Am. Chem. Soc.* **1981**, *103*, 5241−5242.
(37) Coutts, S. J.; Adams, J.; Krolikowski, D.; Snow, R. J. Two efficient methods for the cleavage of pinanediol boronate esters yielding the free boronic acids. *Tetrahedron Lett.* **1994**, *35*, 5109−5112.
(38) Bross, P. F.; Kane, R.; Farrell, A. T.; Abraham, S.; Benson, K.; Brower, M. E.; Bradley, S.; Gobburu, J. V.; Goheer, A.; Lee, S. L.; Leighton, J.; Liang, C. Y.; Lostritto, R. T.; McGuinn, W. D.; Morse, D. E.; Rahman, A.; Rosario, L. A.; Verbois, S. L.; Williams, G.; Wang, Y. C.; Pazdur, R. Approval summary for bortezomib for injection in the treatment of multiple myeloma. *Clin. Cancer Res.* **2004**, *10*, 3954−3964.
(39) Welter, J.; Kavanagh, P.; Meyer, M. R.; Maurer, H. H. Benzofuran analogues of amphetamine and methamphetamine:

studies on the metabolism and toxicological analysis of 5-APB and 5-MAPB in urine and plasma using GC-MS and LC-(HR)-MS^n techniques. *Anal. Bioanal. Chem.* **2015**, *407*, 1371−1388.

(40) Klein, M.; Busch, M.; Esdar, C.; Friese-Hamim, M.; Krier, M.; Musil, D.; Rohdich, F.; Sanderson, M.; Walter, G.; Schadt, O.; Zanelli, U.; Ma, J. Abstract LB-054: Discovery and profiling of M3258, a potent and selective LMP7 inhibitor demonstrating high efficacy in multiple myeloma models. *Cancer Res.* **2019**, *79*, LB-054.

(41) Sanderson, M.; Busch, M.; Esdar, C.; Friese-Hamim, M.; Krier, M.; Ma, J.; Musil, D.; Rohdich, F.; Sloot, W.; Walter, G.; Zanelli, U.; Schadt, O.; Klein, M. Abstract DDT02-01: First-time disclosure of M3258: a selective inhibitor of the immunoproteasome subunit LMP7 with potential for improved therapeutic utility in multiple myeloma compared to pan-proteasome inhibitors. *Cancer Res.* **2019**, *79*, DDT02−01.

(42) Sanderson, M. P.; Friese-Hamim, M.; Walter-Bausch, G.; Busch, M.; Gaus, S.; Musil, D.; Rohdich, F.; Zanelli, U.; Downey-Kopyscinski, S. L.; Mitsiades, C. S.; Schadt, O.; Klein, M.; Esdar, C. M3258 is a selective inhibitor of the immunoproteasome subunit LMP7 (β5i) delivering efficacy in multiple myeloma models. *Mol. Cancer Ther.* **2021**, DOI: 10.1158/1535-7163.MCT-21-0005.

(43) Couper, F. J.; Marinetti, L. J. γ-hydroxybutyrate (GHB)—effects on human performance and behavior. *Forensic Sci. Rev.* **2002**, *14*, 101−121.

(44) Engel, D.; Nudelman, A.; Tarasenko, N.; Levovich, I.; Makarovsky, I.; Sochotnikov, S.; Tarasenko, I.; Rephaeli, A. Novel prodrugs of tegafur that display improved anticancer activity and antiangiogenic properties. *J. Med. Chem.* **2008**, *51*, 314−323.

(45) Menhaji-Klotz, E.; Hesp, K. D.; Londregan, A. T.; Kalgutkar, A. S.; Piotrowski, D. W.; Boehm, M.; Song, K.; Ryder, T.; Beaumont, K.; Jones, R. M.; Atkinson, K.; Brown, J. A.; Litchfield, J.; Xiao, J.; Canterbury, D. P.; Burford, K.; Thuma, B. A.; Limberakis, C.; Jiao, W.; Bagley, S. W.; Agarwal, S.; Crowell, D.; Pazdziorko, S.; Ward, J.; Price, D. A.; Clerin, V. Discovery of a novel small-molecule modulator of C-X-C chemokine receptor type 7 as a treatment for cardiac fibrosis. *J. Med. Chem.* **2018**, *61*, 3685−3696.

(46) Sula Karreci, E.; Fan, H.; Uehara, M.; Mihali, A. B.; Singh, P. K.; Kurdi, A. T.; Solhjou, Z.; Riella, L. V.; Ghobrial, I.; Laragione, T.; Routray, S.; Assaker, J. P.; Wang, R.; Sukenick, G.; Shi, L.; Barrat, F. J.; Nathan, C. F.; Lin, G.; Azzi, J. Brief treatment with a highly selective immunoproteasome inhibitor promotes long-term cardiac allograft acceptance in mice. *Proc. Natl. Acad. Sci. U. S. A.* **2016**, *113*, E8425−E8432.

(47) Dechavanne, V.; Vilbois, F.; Glez, L.; Antonsson, B. Purification and separation of the 20S immunoproteasome from the constitutive proteasome and identification of the subunits by LC-MS. *Protein Expression Purif.* **2013**, *87*, 100−110.

(48) Parlati, F.; Lee, S. J.; Aujay, M.; Suzuki, E.; Levitsky, K.; Lorens, J. B.; Micklem, D. R.; Ruurs, P.; Sylvain, C.; Lu, Y.; Shenk, K. D.; Bennett, M. K. Carfilzomib can induce tumor cell death through selective inhibition of the chymotrypsin-like activity of the proteasome. *Blood* **2009**, *114*, 3439−3447.

(49) Collaborative Computational Project, N. The CCP4 suite: programs for protein crystallography. *Acta Crystallogr., Sect. D: Biol. Crystallogr.* **1994**, *50*, 760−763.

(50) Unno, M.; Mizushima, T.; Morimoto, Y.; Tomisugi, Y.; Tanaka, K.; Yasuoka, N.; Tsukihara, T. The structure of the mammalian 20S proteasome at 2.75 Å resolution. *Structure* **2002**, *10*, 609−618.

(51) Emsley, P.; Cowtan, K. Coot: model-building tools for molecular graphics. *Acta Crystallogr., Sect. D: Biol. Crystallogr.* **2004**, *60*, 2126−2132.

(52) Bricogne, G.; Blanc, E.; Brandl, M.; Flensburg, C.; Keller, P.; Paciorek, W.; Roversi, P.; Sharff, A.; Smart, O. S.; Vonrhein, C.; Womack, T. O. *BUSTER version 2.11.7* Global Phasing Ltd: Cambridge, United Kingdom.

https://doi.org/10.1021/acs.jmedchem.1c00604
J. Med. Chem. 2021, 64, 10230−10245